SLAC-PUB-15866
arXiv:1312.5364

Measurement of the $B \to X_s \ell^+ \ell^-$ branching fraction and search for direct CP violation from a sum of exclusive final states

J. P. Lees,[1] V. Poireau,[1] V. Tisserand,[1] E. Grauges,[2] A. Palano[ab],[3] G. Eigen,[4] B. Stugu,[4] D. N. Brown,[5] L. T. Kerth,[5] Yu. G. Kolomensky,[5] M. J. Lee,[5] G. Lynch,[5] H. Koch,[6] T. Schroeder,[6] C. Hearty,[7] T. S. Mattison,[7] J. A. McKenna,[7] R. Y. So,[7] A. Khan,[8] V. E. Blinov[ac],[9] A. R. Buzykaev[a],[9] V. P. Druzhinin[ab],[9] V. B. Golubev[ab],[9] E. A. Kravchenko[ab],[9] A. P. Onuchin[ac],[9] S. I. Serednyakov[ab],[9] Yu. I. Skovpen[ab],[9] E. P. Solodov[ab],[9] K. Yu. Todyshev[ab],[9] A. N. Yushkov[a],[9] A. J. Lankford,[10] M. Mandelkern,[10] B. Dey,[11] J. W. Gary,[11] O. Long,[11] C. Campagnari,[12] M. Franco Sevilla,[12] T. M. Hong,[12] D. Kovalskyi,[12] J. D. Richman,[12] C. A. West,[12] A. M. Eisner,[13] W. S. Lockman,[13] B. A. Schumm,[13] A. Seiden,[13] D. S. Chao,[14] C. H. Cheng,[14] B. Echenard,[14] K. T. Flood,[14] D. G. Hitlin,[14] T. S. Miyashita,[14] P. Ongmongkolkul,[14] F. C. Porter,[14] R. Andreassen,[15] Z. Huard,[15] B. T. Meadows,[15] B. G. Pushpawela,[15] M. D. Sokoloff,[15] L. Sun,[15] P. C. Bloom,[16] W. T. Ford,[16] A. Gaz,[16] U. Nauenberg,[16] J. G. Smith,[16] S. R. Wagner,[16] R. Ayad,[17,*] W. H. Toki,[17] B. Spaan,[18] R. Schwierz,[19] D. Bernard,[20] M. Verderi,[20] S. Playfer,[21] D. Bettoni[a],[22] C. Bozzi[a],[22] R. Calabrese[ab],[22] G. Cibinetto[ab],[22] E. Fioravanti[ab],[22] I. Garzia[ab],[22] E. Luppi[ab],[22] L. Piemontese[a],[22] V. Santoro[a],[22] A. Calcaterra,[23] R. de Sangro,[23] G. Finocchiaro,[23] S. Martellotti,[23] P. Patteri,[23] I. M. Peruzzi,[23,†] M. Piccolo,[23] M. Rama,[23] A. Zallo,[23] R. Contri[ab],[24] E. Guido[ab],[24] M. Lo Vetere[ab],[24] M. R. Monge[ab],[24] S. Passaggio[a],[24] C. Patrignani[ab],[24] E. Robutti[a],[24] B. Bhuyan,[25] V. Prasad,[25] M. Morii,[26] A. Adametz,[27] U. Uwer,[27] H. M. Lacker,[28] P. D. Dauncey,[29] U. Mallik,[30] C. Chen,[31] J. Cochran,[31] W. T. Meyer,[31] S. Prell,[31] H. Ahmed,[32] A. V. Gritsan,[33] N. Arnaud,[34] M. Davier,[34] D. Derkach,[34] G. Grosdidier,[34] F. Le Diberder,[34] A. M. Lutz,[34] B. Malaescu,[34,‡] P. Roudeau,[34] A. Stocchi,[34] G. Wormser,[34] D. J. Lange,[35] D. M. Wright,[35] J. P. Coleman,[36] J. R. Fry,[36] E. Gabathuler,[36] D. E. Hutchcroft,[36] D. J. Payne,[36] C. Touramanis,[36] A. J. Bevan,[37] F. Di Lodovico,[37] R. Sacco,[37] G. Cowan,[38] J. Bougher,[39] D. N. Brown,[39] C. L. Davis,[39] A. G. Denig,[40] M. Fritsch,[40] W. Gradl,[40] K. Griessinger,[40] A. Hafner,[40] E. Prencipe,[40] K. R. Schubert,[40] R. J. Barlow,[41,§] G. D. Lafferty,[41] R. Cenci,[42] B. Hamilton,[42] A. Jawahery,[42] D. A. Roberts,[42] R. Cowan,[43] D. Dujmic,[43] G. Sciolla,[43] R. Cheaib,[44] P. M. Patel,[44,¶] S. H. Robertson,[44] P. Biassoni[ab],[45] N. Neri[a],[45] F. Palombo[ab],[45] L. Cremaldi,[46] R. Godang,[46,**] P. Sonnek,[46] D. J. Summers,[46] M. Simard,[47] P. Taras,[47] G. De Nardo[ab],[48] D. Monorchio[ab],[48] G. Onorato[ab],[48] C. Sciacca[ab],[48] M. Martinelli,[49] G. Raven,[49] C. P. Jessop,[50] J. M. LoSecco,[50] K. Honscheid,[51] R. Kass,[51] J. Brau,[52] R. Frey,[52] N. B. Sinev,[52] D. Strom,[52] E. Torrence,[52] E. Feltresi[ab],[53] M. Margoni[ab],[53] M. Morandin[a],[53] M. Posocco[a],[53] M. Rotondo[a],[53] G. Simi[ab],[53] F. Simonetto[ab],[53] R. Stroili[ab],[53] S. Akar,[54] E. Ben-Haim,[54] M. Bomben,[54] G. R. Bonneaud,[54] H. Briand,[54] G. Calderini,[54] J. Chauveau,[54] Ph. Leruste,[54] G. Marchiori,[54] J. Ocariz,[54] S. Sitt,[54] M. Biasini[ab],[55] E. Manoni[a],[55] S. Pacetti[ab],[55] A. Rossi[a],[55] C. Angelini[ab],[56] G. Batignani[ab],[56] S. Bettarini[ab],[56] M. Carpinelli[ab],[56,††] G. Casarosa[ab],[56] A. Cervelli[ab],[56] M. Chrzaszcz[ab],[56] F. Forti[ab],[56] M. A. Giorgi[ab],[56] A. Lusiani[ac],[56] B. Oberhof[ab],[56] E. Paoloni[ab],[56] A. Perez[a],[56] G. Rizzo[ab],[56] J. J. Walsh[a],[56] D. Lopes Pegna,[57] J. Olsen,[57] A. J. S. Smith,[57] R. Faccini[ab],[58] F. Ferrarotto[a],[58] F. Ferroni[ab],[58] M. Gaspero[ab],[58] L. Li Gioi[a],[58] G. Piredda[a],[58] C. Bünger,[59] O. Grünberg,[59] T. Hartmann,[59] T. Leddig,[59] C. Voß,[59] R. Waldi,[59] T. Adye,[60] E. O. Olaiya,[60] F. F. Wilson,[60] S. Emery,[61] G. Hamel de Monchenault,[61] G. Vasseur,[61] Ch. Yèche,[61] F. Anulli,[62,‡‡] D. Aston,[62] D. J. Bard,[62] J. F. Benitez,[62] C. Cartaro,[62] M. R. Convery,[62] J. Dorfan,[62] G. P. Dubois-Felsmann,[62] W. Dunwoodie,[62] M. Ebert,[62] R. C. Field,[62] B. G. Fulsom,[62] A. M. Gabareen,[62] M. T. Graham,[62] C. Hast,[62] W. R. Innes,[62] P. Kim,[62] M. L. Kocian,[62] D. W. G. S. Leith,[62] P. Lewis,[62] D. Lindemann,[62] B. Lindquist,[62] S. Luitz,[62] V. Luth,[62] H. L. Lynch,[62] D. B. MacFarlane,[62] D. R. Muller,[62] H. Neal,[62] S. Nelson,[62] M. Perl,[62] T. Pulliam,[62] B. N. Ratcliff,[62] A. Roodman,[62] A. A. Salnikov,[62] R. H. Schindler,[62] A. Snyder,[62] D. Su,[62] M. K. Sullivan,[62] J. Va'vra,[62] A. P. Wagner,[62] W. F. Wang,[62] W. J. Wisniewski,[62] M. Wittgen,[62] D. H. Wright,[62] H. W. Wulsin,[62] V. Ziegler,[62] W. Park,[63] M. V. Purohit,[63] R. M. White,[63,§§] J. R. Wilson,[63] A. Randle-Conde,[64] S. J. Sekula,[64] M. Bellis,[65] P. R. Burchat,[65] E. M. T. Puccio,[65] M. S. Alam,[66] J. A. Ernst,[66] R. Gorodeisky,[67] N. Guttman,[67] D. R. Peimer,[67] A. Soffer,[67] S. M. Spanier,[68] J. L. Ritchie,[69] A. M. Ruland,[69] R. F. Schwitters,[69] B. C. Wray,[69] J. M. Izen,[70] X. C. Lou,[70] F. Bianchi[ab],[71] F. De Mori[ab],[71] A. Filippi[a],[71] D. Gamba[ab],[71]

S. Zambito[ab],[71] L. Lanceri[ab],[72] L. Vitale[ab],[72] F. Martinez-Vidal,[73] A. Oyanguren,[73] P. Villanueva-Perez,[73] J. Albert,[74] Sw. Banerjee,[74] F. U. Bernlochner,[74] H. H. F. Choi,[74] G. J. King,[74] R. Kowalewski,[74] M. J. Lewczuk,[74] T. Lueck,[74] I. M. Nugent,[74] J. M. Roney,[74] R. J. Sobie,[74] N. Tasneem,[74] T. J. Gershon,[75] P. F. Harrison,[75] T. E. Latham,[75] H. R. Band,[76] S. Dasu,[76] Y. Pan,[76] R. Prepost,[76] and S. L. Wu[76]

(The *BABAR* Collaboration)

[1]*Laboratoire d'Annecy-le-Vieux de Physique des Particules (LAPP), Université de Savoie, CNRS/IN2P3, F-74941 Annecy-Le-Vieux, France*
[2]*Universitat de Barcelona, Facultat de Fisica, Departament ECM, E-08028 Barcelona, Spain*
[3]*INFN Sezione di Bari[a]; Dipartimento di Fisica, Università di Bari[b], I-70126 Bari, Italy*
[4]*University of Bergen, Institute of Physics, N-5007 Bergen, Norway*
[5]*Lawrence Berkeley National Laboratory and University of California, Berkeley, California 94720, USA*
[6]*Ruhr Universität Bochum, Institut für Experimentalphysik 1, D-44780 Bochum, Germany*
[7]*University of British Columbia, Vancouver, British Columbia, Canada V6T 1Z1*
[8]*Brunel University, Uxbridge, Middlesex UB8 3PH, United Kingdom*
[9]*Budker Institute of Nuclear Physics SB RAS, Novosibirsk 630090[a], Novosibirsk State University, Novosibirsk 630090[b], Novosibirsk State Technical University, Novosibirsk 630092[c], Russia*
[10]*University of California at Irvine, Irvine, California 92697, USA*
[11]*University of California at Riverside, Riverside, California 92521, USA*
[12]*University of California at Santa Barbara, Santa Barbara, California 93106, USA*
[13]*University of California at Santa Cruz, Institute for Particle Physics, Santa Cruz, California 95064, USA*
[14]*California Institute of Technology, Pasadena, California 91125, USA*
[15]*University of Cincinnati, Cincinnati, Ohio 45221, USA*
[16]*University of Colorado, Boulder, Colorado 80309, USA*
[17]*Colorado State University, Fort Collins, Colorado 80523, USA*
[18]*Technische Universität Dortmund, Fakultät Physik, D-44221 Dortmund, Germany*
[19]*Technische Universität Dresden, Institut für Kern- und Teilchenphysik, D-01062 Dresden, Germany*
[20]*Laboratoire Leprince-Ringuet, Ecole Polytechnique, CNRS/IN2P3, F-91128 Palaiseau, France*
[21]*University of Edinburgh, Edinburgh EH9 3JZ, United Kingdom*
[22]*INFN Sezione di Ferrara[a]; Dipartimento di Fisica e Scienze della Terra, Università di Ferrara[b], I-44122 Ferrara, Italy*
[23]*INFN Laboratori Nazionali di Frascati, I-00044 Frascati, Italy*
[24]*INFN Sezione di Genova[a]; Dipartimento di Fisica, Università di Genova[b], I-16146 Genova, Italy*
[25]*Indian Institute of Technology Guwahati, Guwahati, Assam, 781 039, India*
[26]*Harvard University, Cambridge, Massachusetts 02138, USA*
[27]*Universität Heidelberg, Physikalisches Institut, D-69120 Heidelberg, Germany*
[28]*Humboldt-Universität zu Berlin, Institut für Physik, D-12489 Berlin, Germany*
[29]*Imperial College London, London, SW7 2AZ, United Kingdom*
[30]*University of Iowa, Iowa City, Iowa 52242, USA*
[31]*Iowa State University, Ames, Iowa 50011-3160, USA*
[32]*Physics Department, Jazan University, Jazan 22822, Kingdom of Saudia Arabia*
[33]*Johns Hopkins University, Baltimore, Maryland 21218, USA*
[34]*Laboratoire de l'Accélérateur Linéaire, IN2P3/CNRS et Université Paris-Sud 11, Centre Scientifique d'Orsay, F-91898 Orsay Cedex, France*
[35]*Lawrence Livermore National Laboratory, Livermore, California 94550, USA*
[36]*University of Liverpool, Liverpool L69 7ZE, United Kingdom*
[37]*Queen Mary, University of London, London, E1 4NS, United Kingdom*
[38]*University of London, Royal Holloway and Bedford New College, Egham, Surrey TW20 0EX, United Kingdom*
[39]*University of Louisville, Louisville, Kentucky 40292, USA*
[40]*Johannes Gutenberg-Universität Mainz, Institut für Kernphysik, D-55099 Mainz, Germany*
[41]*University of Manchester, Manchester M13 9PL, United Kingdom*
[42]*University of Maryland, College Park, Maryland 20742, USA*
[43]*Massachusetts Institute of Technology, Laboratory for Nuclear Science, Cambridge, Massachusetts 02139, USA*
[44]*McGill University, Montréal, Québec, Canada H3A 2T8*
[45]*INFN Sezione di Milano[a]; Dipartimento di Fisica, Università di Milano[b], I-20133 Milano, Italy*
[46]*University of Mississippi, University, Mississippi 38677, USA*
[47]*Université de Montréal, Physique des Particules, Montréal, Québec, Canada H3C 3J7*
[48]*INFN Sezione di Napoli[a]; Dipartimento di Scienze Fisiche, Università di Napoli Federico II[b], I-80126 Napoli, Italy*
[49]*NIKHEF, National Institute for Nuclear Physics and High Energy Physics, NL-1009 DB Amsterdam, The Netherlands*
[50]*University of Notre Dame, Notre Dame, Indiana 46556, USA*
[51]*Ohio State University, Columbus, Ohio 43210, USA*
[52]*University of Oregon, Eugene, Oregon 97403, USA*

[53] INFN Sezione di Padova[a]; Dipartimento di Fisica, Università di Padova[b], I-35131 Padova, Italy
[54] Laboratoire de Physique Nucléaire et de Hautes Energies, IN2P3/CNRS, Université Pierre et Marie Curie-Paris6, Université Denis Diderot-Paris7, F-75252 Paris, France
[55] INFN Sezione di Perugia[a]; Dipartimento di Fisica, Università di Perugia[b], I-06123 Perugia, Italy
[56] INFN Sezione di Pisa[a]; Dipartimento di Fisica, Università di Pisa[b]; Scuola Normale Superiore di Pisa[c], I-56127 Pisa, Italy
[57] Princeton University, Princeton, New Jersey 08544, USA
[58] INFN Sezione di Roma[a]; Dipartimento di Fisica, Università di Roma La Sapienza[b], I-00185 Roma, Italy
[59] Universität Rostock, D-18051 Rostock, Germany
[60] Rutherford Appleton Laboratory, Chilton, Didcot, Oxon, OX11 0QX, United Kingdom
[61] CEA, Irfu, SPP, Centre de Saclay, F-91191 Gif-sur-Yvette, France
[62] SLAC National Accelerator Laboratory, Stanford, California 94309 USA
[63] University of South Carolina, Columbia, South Carolina 29208, USA
[64] Southern Methodist University, Dallas, Texas 75275, USA
[65] Stanford University, Stanford, California 94305-4060, USA
[66] State University of New York, Albany, New York 12222, USA
[67] Tel Aviv University, School of Physics and Astronomy, Tel Aviv, 69978, Israel
[68] University of Tennessee, Knoxville, Tennessee 37996, USA
[69] University of Texas at Austin, Austin, Texas 78712, USA
[70] University of Texas at Dallas, Richardson, Texas 75083, USA
[71] INFN Sezione di Torino[a]; Dipartimento di Fisica, Università di Torino[b], I-10125 Torino, Italy
[72] INFN Sezione di Trieste[a]; Dipartimento di Fisica, Università di Trieste[b], I-34127 Trieste, Italy
[73] IFIC, Universitat de Valencia-CSIC, E-46071 Valencia, Spain
[74] University of Victoria, Victoria, British Columbia, Canada V8W 3P6
[75] Department of Physics, University of Warwick, Coventry CV4 7AL, United Kingdom
[76] University of Wisconsin, Madison, Wisconsin 53706, USA

We measure the total branching fraction of the flavor-changing neutral-current process $B \to X_s\,\ell^+\ell^-$, along with partial branching fractions in bins of dilepton and hadronic system (X_s) mass, using a sample of 471×10^6 $\Upsilon(4S) \to B\overline{B}$ events recorded with the *BABAR* detector. The admixture of charged and neutral B mesons produced at PEP-II are reconstructed by combining a dilepton pair with 10 different X_s final states. Extrapolating from a sum over these exclusive modes, we measure a lepton-flavor-averaged inclusive branching fraction $\mathcal{B}(B \to X_s\,\ell^+\ell^-) = \left(6.73^{+0.70}_{-0.64}[\text{stat}]^{+0.34}_{-0.25}[\text{exp syst}] \pm 0.50[\text{model syst}]\right) \times 10^{-6}$ for $m^2_{\ell^+\ell^-} > 0.1\,\text{GeV}^2/c^4$. Restricting our analysis exclusively to final states from which a decaying B meson's flavor can be inferred, we additionally report measurements of the direct CP asymmetry A_{CP} in bins of dilepton mass; over the full dilepton mass range, we find $A_{CP} = 0.04 \pm 0.11 \pm 0.01$ for a lepton-flavor-averaged sample.

PACS numbers: 13.20.He, 12.15.-y, 11.30.Er

The $b \to s\ell^+\ell^-$ transition, where b is a bottom quark, s is a strange quark, and $\ell^+\ell^-$ is an e^+e^- or $\mu^+\mu^-$ pair, is forbidden at lowest order in the standard model (SM) but is allowed at one loop via electroweak penguin and W-box diagrams. The amplitude for this decay is expressed in terms of perturbatively calculable effective Wilson coefficients, C_7^{eff}, C_9^{eff}, and C_{10}^{eff}, which represent the electromagnetic penguin diagram, and the vector part and the axial-vector part of the linear combination of the Z penguin and W^+W^- box diagrams, respectively [1]. Non-SM contributions can enter these loops at the same order as the SM processes, modifying the Wilson coefficients from their SM expectations and allowing experimental sensitivity to possible non-SM physics [2–11].

We study the inclusive decay $B \to X_s\,\ell^+\ell^-$, where X_s is a hadronic system containing exactly one kaon, using a sum over exclusive final states, which provides a basis for extrapolation to the fully inclusive rate. We measure the total branching fraction (BF), as well as partial BFs in five disjoint dilepton mass-squared $q^2 \equiv m^2_{\ell^+\ell^-}$ bins and four hadronic mass m_{X_s} bins, which are defined in Table I. We additionally search for direct CP violation in the same q^2 bins. The relative precision of our results is approximately a factor of two better than the combined precision of all similar previously published measurements [12].

The X_s system in the lowest mass m_{X_s} bin $m_{X_s,1}$ contains a single kaon with no other hadrons present; the $m_{X_s,2}$ bin is populated only above the $K\pi$ threshold. Results are also reported in an additional q^2 region $q_0^2 \equiv 1 < q^2 < 6\,\text{GeV}^2/c^4$, i.e., the perturbative window away from the photon pole at low q^2 and the $c\overline{c}$ resonances at higher q^2, where theory uncertainties are well controlled [13–24]. The most recent SM predictions in this region are $\mathcal{B}^{\text{low}}(B \to X_s\,\mu^+\mu^-) = (1.59 \pm 0.11) \times 10^{-6}$ and $\mathcal{B}^{\text{low}}(B \to X_s\,e^+e^-) = (1.64 \pm 0.11) \times 10^{-6}$ [22].

Theory uncertainties in the q^2 range above the $\psi(2S)$ are also well-characterized but relatively much larger than above, with SM predictions for $q^2 > 14.4\,\mathrm{GeV}^2/c^4$ of $\mathcal{B}^{\rm high}(B \to X_s\,\mu^+\mu^-) = (0.24 \pm 0.07) \times 10^{-6}$ and $\mathcal{B}^{\rm high}(B \to X_s\,e^+e^-) = (0.21 \pm 0.07) \times 10^{-6}$ [22]. The SM expectation in the $q^2 > 4m_\mu^2$ range is $\mathcal{B}(B \to X_s\,\ell^+\ell^-) = (4.6 \pm 0.8) \times 10^{-6}$ [20]. Direct *CP* violation, defined as $A_{CP} \equiv (\mathrm{BF}_{\overline{b}} - \mathrm{BF}_b)/(\mathrm{BF}_{\overline{b}} + \mathrm{BF}_b)$, where b ($\overline{b}$) denotes a $\overline{B}$ (B) parent, is expected to be suppressed well below the 1% level in both exclusive and inclusive $b \to s\ell^+\ell^-$ transitions [25–28]; however, in beyond-SM models with four quark generations, significant enhancements are possible, particularly in the high-q^2 region [10, 11].

The *BABAR* [29] and Belle [30] Collaborations have previously published $B \to X_s\,\ell^+\ell^-$ BFs based on a sum over exclusive final states using only $\sim 25\%$ of each experiment's final dataset. More recently, both collaborations (along with LHCb and CDF) have published BFs, and time-integrated rate and angular asymmetries, for the exclusive decays $B \to K^{(*)}\ell^+\ell^-$ [31–37]. The present analysis uses the $424.2 \pm 1.8\,\mathrm{fb}^{-1}$ $e^+e^- \to \Upsilon(4S)$ data sample [38], corresponding to ~ 471 million $B\overline{B}$ pairs, collected with the *BABAR* detector [39, 40] at the PEP-II collider at the SLAC National Accelerator Laboratory.

The decays $B \to X_s\,\ell^+\ell^-$ are reconstructed in 10 separate X_s hadronic final states (K^+, $K^+\pi^0$, $K^+\pi^-$, $K^+\pi^-\pi^0$, $K^+\pi^-\pi^+$, K^0_S, $K^0_S\pi^0$, $K^0_S\pi^+$, $K^0_S\pi^+\pi^0$, and $K^0_S\pi^+\pi^-$) [41], combining these with an e^+e^- or $\mu^+\mu^-$ pair for a total of 20 final states. The selection of charged and neutral particle candidates, as well as the reconstruction of $\pi^0 \to \gamma\gamma$ and $K^0_S \to \pi^+\pi^-$, is described in Refs. [31, 36]. Based on studies including up to 18 X_s modes with a maximum of four pions and m_{X_s} as large as $2.2\,\mathrm{GeV}/c^2$, we limit the number of X_s final states to the 10 listed above and require $m_{X_s} < 1.8\,\mathrm{GeV}/c^2$ since the expected signal-to-background ratio rapidly decreases with increasing X_s pion multiplicity and mass. We assume that the fraction of modes containing a K^0_L is equal to that containing a K^0_S and account for these decays, as well as $K^0_S \to \pi^0\pi^0$ and π^0 Dalitz decays, in our reconstruction efficiencies. With these efficiencies taken into account, the reconstructed states represent $\sim 70\%$ of the total inclusive rate.

We account for missing hadronic final states, as well as for states with $m_{X_s} > 1.8\,\mathrm{GeV}/c^2$, based on the formalism of Refs. [8, 13, 22, 42–44], with hadronization of the X_s system provided by the JETSET [45] event generator. Given that we observe no statistically significant nonresonant $B \to K\pi\ell^+\ell^-$ decays in our data [31], signal decays with a two-body X_s system and $m_{X_s} < 1.1\,\mathrm{GeV}/c^2$ are assumed to proceed through the $K^*(892)$ resonance. The simulation of such events, as well as those with a single kaon and no pions, is similar to that for inclusive events but incorporates the form factor models of Refs. [46, 47].

The kinematic variables $m_{\rm ES} = \sqrt{E^2_{\rm CM}/4 - p^{*2}_B}$ and $\Delta E = E^*_B - E_{\rm CM}/2$, where p^*_B and E^*_B are the B momentum and energy in the $\Upsilon(4S)$ center-of-mass (CM) frame with $E_{\rm CM}$ the total CM energy, are used to distinguish signal from background events. We require $m_{\rm ES} > 5.225\,\mathrm{GeV}/c^2$ and $-0.10 < \Delta E < 0.05\,\mathrm{GeV}$ ($-0.05 < \Delta E < 0.05\,\mathrm{GeV}$) for dielectron (dimuon) final states. Signal-like B backgrounds with J/ψ ($\psi(2S)$) daughters are removed by vetoing events with $6.8 < q^2 < 10.1\,\mathrm{GeV}^2/c^4$ ($12.9 < q^2 < 14.2$). We reconstruct $X_s h^\pm \mu^\mp$ final states, where h is a track with no particle identification (PID) requirement applied, to characterize backgrounds from hadrons misidentified as muons. Such backgrounds occur only in dimuon final states because of the significantly higher probability to misidentify K^+ or π^+ as a muon rather than an electron. Similarly, backgrounds from $B \to D(\to K^{(*)}\pi)\pi$ decays occur only in dimuon modes and, assigning the pion mass hypothesis to both muon candidates, we reject candidates with $K^{(*)}\pi$ mass values in the range $1.84 < m_{K^{(*)}\pi} < 2.04\,\mathrm{GeV}/c^2$.

We suppress $e^+e^- \to q\overline{q}$ events (where q is a u, d, s or c quark) and $B\overline{B}$ combinatoric backgrounds using boosted decision trees (BDTs) [48, 49] identical in construction to those used in our $B \to K^{(*)}\ell^+\ell^-$ analysis [31]. These BDTs are respectively trained with simulated $udsc$ or $B\overline{B}$ backgrounds and correctly reconstructed signal events. Ensembles of simulated event samples are used to simultaneously optimize the ΔE windows and selection on the $udsc$ BDTs for each individual q^2 and m_{X_s} bin. After all selection criteria are applied, the average multiplicity of B candidates per event is $\approx$2.6 ($\approx$2.2) for e^+e^- ($\mu^+\mu^-$) final states. We allow only one candidate per event, selecting the candidate with the smallest $|\Delta E|$. Signal efficiencies after event selection range from about 1 to 30% depending on mode and the q^2 or m_{X_s} bin.

In each q^2 and m_{X_s} bin, we extract the signal yield with a two-dimensional maximum likelihood (ML) fit using $m_{\rm ES}$ and a likelihood ratio L_R based on the $B\overline{B}$ BDT, $L_R \equiv \mathcal{P}_{\rm S}/(\mathcal{P}_{\rm S} + \mathcal{P}_{\rm B})$, where $\mathcal{P}_{\rm S}$ and $\mathcal{P}_{\rm B}$ are, respectively, probabilities for genuine-signal and $B\overline{B}$ backgrounds. For correctly reconstructed signal events, L_R sharply peaks near one, while $B\overline{B}$ backgrounds peak at zero. Events with $L_R > 0.42$ are selected. This selection rejects $\gtrsim 95\%$ of the $B\overline{B}$ background events remaining after all other event selections have been applied, with only a trivial reduction in signal efficiency.

Five (six) event classes contribute to the dielectron (dimuon) ML fit: (1) correctly reconstructed signal; (2) events that contain a partially or incorrectly reconstructed $B \to X_s\,\ell^+\ell^-$ decay (signal cross-feed); (3) $udsc$ and (4) $B\overline{B}$ combinatorial backgrounds; (5) charmonium backgrounds; and, for dimuon modes, (6) events with hadrons misidentified as muons.

There is no correlation between $m_{\rm ES}$ and L_R for correctly reconstructed signal events. Therefore, the probability distribution function (PDF) for these events is chosen as a product of two one-dimensional (1D) PDFs,

with $m_{\rm ES}$ parameterized with a Crystal Ball (CB) function [50–52] and L_R described by a non-parametric histogram PDF. The CB shape parameters are fixed using simulated signal events, as is the L_R PDF. These PDFs describe well the $m_{\rm ES}$ and L_R distributions derived from the high-statistics control samples of vetoed signal-like charmonium events. The signal cross-feed is modeled as a two-dimensional (2D) $m_{\rm ES}$ versus L_R histogram PDF using simulated signal samples, with normalization $N_{\rm xfd}$ scaled as a fixed fraction of the fit signal yield $N_{\rm sig}$.

The *udsc* combinatoric background PDF is derived from simulated events using a 2D non-parametric kernel density estimator with adaptive bandwidth [49, 53, 54], which is validated using data collected with e^+e^- center-of-mass energy 40 MeV below the $\Upsilon(4S)$ resonance. The *udsc* normalization $N_{\rm udsc}$ is obtained by scaling the $43.9 \pm 0.2\,{\rm fb}^{-1}$ of off-resonance data [38] by the ratio of on- to off-resonance integrated luminosity.

The shape of the 2D PDF for the $B\overline{B}$ combinatoric background is modeled similarly to the *udsc* background. Its normalization in the $5.225 < m_{\rm ES} < 5.270\,{\rm GeV}/c^2$ sideband, where no correctly reconstructed signal events are expected, is obtained by subtracting the $N^{\rm SB}_{\rm xfd}$, $N^{\rm SB}_{\rm udsc}$, $N^{\rm SB}_{\rm chm}$ and $N^{\rm SB}_{\rm had}$ (for dimuon events) contributions from the total number of sideband events, giving the $B\overline{B}$ yield in the sideband region $N^{\rm SB}_{B\overline{B}}$. We use simulated events to obtain the ratio of the number of $B\overline{B}$ combinatoric events in the $m_{\rm ES} > 5.27\,{\rm GeV}/c^2$ signal region to the number in the sideband region to scale $N^{\rm SB}_{B\overline{B}}$ into the expected contribution $N_{B\overline{B}}$ in the full fit region.

Charmonium backgrounds escaping the vetoed q^2 regions are similarly described by a 2D kernel estimator, with normalization $N_{\rm chm}$ derived from a fit to the data in the vetoed regions that is extrapolated into the non-vetoed regions. The normalization $N_{\rm had}$ and shape of the 2D PDF for misidentified dimuon events are characterized by a weighted 2D histogram taken directly from data using event-by-event weights obtained from PID control samples [31, 55].

We extract the $N_{\rm sig}$ central value and associated upper and lower limits using the negative log-likelihood (NLL) for $N_{\rm sig}$. We calculate partial BFs taking into account the efficiency for each final state in each q^2 and m_{X_s} bin, as well as the multiplicative factors that provide extrapolation to the fully inclusive BFs. The results are shown in Table I, where the fully inclusive total rate and the m_{X_s} binned results include estimated signal contributions in the vetoed charmonium q^2 regions. Fit projections for all q^2 and m_{X_s} bins are available as supplemental EPAPS material [56], along with a table giving the raw numerical results from our fits. Figure 1 shows our q^2 binned results overlaid on the nominal SM expectations derived from our $B \to X_s\,\ell^+\ell^-$ signal model. A similar plot for m_{X_s} is included as supplemental material.

We consider systematic uncertainties associated with purely experimental systematic uncertainties and the model-dependent extrapolation to the fully inclusive rate. The experimental systematics can either be additive, affecting the extraction of the signal yield from the data, or multiplicative, affecting the calculation of a BF from an observed signal yield. Sources of multiplicative systematic uncertainty include $B\overline{B}$ counting as well as tracking, PID and reconstruction efficiencies. The only significant additive systematic uncertainties are associated with the PDF parameterizations and normalizations. The total experimental systematic uncertainty is the sum-in-quadrature of the above terms, with the exception that uncertainties related to charged particle tracking efficiencies are assumed to be fully correlated among all charged particles. The evaluation of all experimental systematics is fully described in Ref. [31]. Tables quantifying each individual contribution to the experimental and model-dependent extrapolation systematic uncertainties are available as supplemental EPAPS material [56].

The uncertainty in the extrapolation to the inclusive rate is characterized through variations that attempt to quantify our lack of knowledge of the true dilepton mass-squared distribution and hadronization of the X_s system beyond the specific final states and m_{X_s} range that we observe. We average the most recent $B \to K^{(*)}\ell^+\ell^-$ BFs [57], excluding *BABAR* results, and use the latest *BABAR* result [58] for the ratio of charged-to-neutral $\Upsilon(4S) \to b\overline{b}$ decays, $\Gamma(B^+B^-)/\Gamma(B^0\overline{B}^0) = 1.006 \pm 0.036 \pm 0.031$. Each of these terms is varied by its one-standard-deviation uncertainty. We examine an alternate m_{X_s} transition point of $1.0\,{\rm GeV}/c^2$ between the $B \to K^{(*)}\ell^+\ell^-$ and $B \to X_s\,\ell^+\ell^-$ models. To account for hadronization uncertainties in $m_{X_s} > 1.1\,{\rm GeV}/c^2$ events, we generate 20 simulated datasets with varied JETSET tunings, two different values for the B-meson Fermi motion, and two different b-quark mass values. We take the full spread of the extrapolation factors derived from these variations to estimate this systematic uncertainty. Additionally, for $m_{X_s} > 1.1\,{\rm GeV}/c^2$, the fraction of modes with more than one π^0 is varied around the generator value of 0.20 by $\pm 50\%$; the fraction of modes with either no π^0 and more than two charged pions, or one π^0 and more than one charged pion, is varied by $\pm 50\%$ around the q^2-dependent generator value; and the fraction of modes with more than one neutral or charged kaon is varied around the generator value of 0.034 by $\pm 50\%$. Contributions from final states with photons that do not come from π^0 decays but rather from η, η', ω, etc., are expected to be insignificant, and we do not vary the fractions of these decays. Each of the above variations is added in quadrature to obtain the final model-dependent systematic. Table I lists both the experimental and model-dependent systematics.

We calculate the total inclusive rate by summing the q^2_1 through q^2_5 results taking into account correlations in the systematic uncertainties and estimating signal contribu-

TABLE I: $B \to X_s\, e^+e^-$, $B \to X_s\, \mu^+\mu^-$ and $B \to X_s\, \ell^+\ell^-$ partial BFs (in units of 10^{-6}) and A_{CP} by $q^2(\,\mathrm{GeV}^2/c^4)$ and $m_{X_s}(\,\mathrm{GeV}/c^2)$ bin. The number in parentheses after each result is the multiplier which is applied to the measured semi-inclusive rate to account for unreconstructed and $m_{X_s} > 1.8\,\mathrm{GeV}/c^2$ final states. Estimated contributions from the vetoed charmonium q^2 regions are included in both the total and m_{X_s} binned results, but not in the total A_{CP}. The first uncertainties are statistical, the second experimental systematics and the third model-dependent systematics associated with the multiplicative factor. There are no model-dependent A_{CP} systematics and A_{CP} is not measured as a function of m_{X_s}; the multiplicative factors are not used in calculating the total A_{CP}.

Bin	Range	$B \to X_s\, e^+e^-$	$B \to X_s\, \mu^+\mu^-$	$B \to X_s\, \ell^+\ell^-$	$A_{CP\,B\to X_s\,\ell^+\ell^-}$
q^2_0	$1.0 < q^2 < 6.0$	$1.93^{+0.47+0.21}_{-0.45-0.16} \pm 0.18$ (1.71)	$0.66^{+0.82+0.30}_{-0.76-0.24} \pm 0.07$ (1.78)	$1.60^{+0.41+0.17}_{-0.39-0.13} \pm 0.18$	$-0.06 \pm 0.22 \pm 0.01$
q^2_1	$0.1 < q^2 < 2.0$	$3.05^{+0.52+0.29}_{-0.49-0.21} \pm 0.35$ (1.96)	$1.83^{+0.90+0.30}_{-0.80-0.24} \pm 0.20$ (2.02)	$2.70^{+0.45+0.21}_{-0.42-0.16} \pm 0.35$	$-0.13 \pm 0.18 \pm 0.01$
q^2_2	$2.0 < q^2 < 4.3$	$0.69^{+0.31+0.11}_{-0.28-0.07} \pm 0.07$ (1.73)	$-0.15^{+0.50+0.26}_{-0.43-0.14} \pm 0.01$ (1.80)	$0.46^{+0.26+0.10}_{-0.23-0.06} \pm 0.07$	$0.42\ ^{+0.50}_{-0.42} \pm 0.01$
q^2_3	$4.3 < q^2 < 6.8$	$0.69^{+0.31+0.13}_{-0.29-0.10} \pm 0.05$ (1.53)	$0.34^{+0.54+0.19}_{-0.50-0.15} \pm 0.03$ (1.59)	$0.60^{+0.27+0.10}_{-0.25-0.08} \pm 0.05$	$-0.45^{+0.44}_{-0.57} \pm 0.01$
q^2_4	$10.1 < q^2 < 12.9$	$1.14^{+0.42+0.22}_{-0.40-0.10} \pm 0.04$ (1.16)	$0.87^{+0.51+0.11}_{-0.47-0.08} \pm 0.03$ (1.18)	$1.02^{+0.32+0.10}_{-0.30-0.07} \pm 0.04$	
q^2_5	$14.2 < q^2$	$0.56^{+0.19+0.03}_{-0.18-0.03} \pm 0.00$ (1.02)	$0.60^{+0.31+0.05}_{-0.29-0.04} \pm 0.00$ (1.02)	$0.57^{+0.16+0.03}_{-0.15-0.02} \pm 0.00$	
q^2_{45}	$q^2_4 \cup q^2_5$	—	—	—	$0.19\ ^{+0.18}_{-0.17} \pm 0.01$
$m_{X_s,1}$	$0.4 < m_{X_s} < 0.6$	$0.69^{+0.18+0.04}_{-0.17-0.03} \pm 0.00$ (1.00)	$0.74^{+0.25+0.04}_{-0.23-0.04} \pm 0.00$ (1.00)	$0.71^{+0.15+0.03}_{-0.14-0.03} \pm 0.00$	
$m_{X_s,2}$	$0.6 < m_{X_s} < 1.0$	$1.20^{+0.34+0.10}_{-0.33-0.07} \pm 0.00$ (1.00)	$0.76^{+0.44+0.08}_{-0.40-0.07} \pm 0.00$ (1.00)	$1.02^{+0.27+0.06}_{-0.25-0.05} \pm 0.00$	
$m_{X_s,3}$	$1.0 < m_{X_s} < 1.4$	$1.60^{+0.72+0.27}_{-0.69-0.19} \pm 0.05$ (1.18)	$0.65^{+1.16+0.27}_{-1.08-0.25} \pm 0.02$ (1.18)	$1.32^{+0.61+0.19}_{-0.58-0.15} \pm 0.05$	
$m_{X_s,4}$	$1.4 < m_{X_s} < 1.8$	$1.88^{+0.76+0.71}_{-0.73-0.47} \pm 0.12$ (1.91)	$0.19^{+1.35+0.70}_{-1.25-0.50} \pm 0.10$ (1.91)	$1.36^{+0.67+0.50}_{-0.63-0.34} \pm 0.12$	
Total	$0.1 < q^2$	$7.69^{+0.82+0.50}_{-0.77-0.33} \pm 0.50$	$4.41^{+1.31+0.57}_{-1.17-0.42} \pm 0.27$	$6.73^{+0.70+0.34}_{-0.64-0.25} \pm 0.50$	$0.04 \pm 0.11 \pm 0.01$

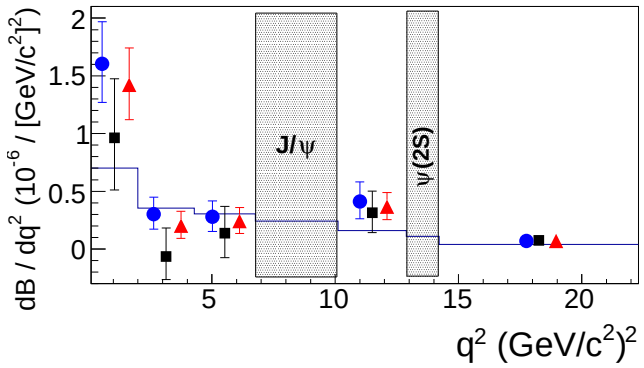

FIG. 1: Differential BF as a function of q^2 for electron (blue circles), muon (black squares) and lepton-flavor-averaged final states (red triangles). The errors correspond to the total uncertainties. The histogram shows the SM expectation, which has uncertainties of approximately 10-30% in different q^2 regions. The shaded boxes denote the vetoed charmonium regions. The horizontal spread of points in each bin is meant only to aid visibility.

tions in the vetoed charmonium q^2 regions. The lepton-flavor-averaged $B \to X_s\, \ell^+\ell^-$ results are weighted averages of the individual $B \to X_s\, e^+e^-$ and $B \to X_s\, \mu^+\mu^-$ results that take into account correlations in the systematic uncertainties. Figure 1 shows the differential BF results as a function of q^2 and m_{X_s} overlaid with the SM expectation. The results in these bins, as well as in the q^2_0 region, are generally in good agreement with SM predictions. Given our experimental uncertainties, we are insensitive to the relatively small differences in the e^+e^- and $\mu^+\mu^-$ rates expected in the SM, and observe no significant differences between e^+e^- and $\mu^+\mu^-$ final states.

Several model-independent analyses of the form-factor-independent angular observables reported in a recent $B^0 \to K^+\pi^-\mu^+\mu^-$ LHCb analysis [35] explain the anomaly reported there in terms of a non-vanishing beyond-SM contribution C_9^{BSM} [59–68]. These phenomenological studies all present generally similar results, yielding a three-sigma range for C_9^{BSM} of $\sim [-2, 0]$, implying a corresponding suppression in the fully inclusive BF of up to $\sim 25\%$ in the $1 < q^2 < 6\,\mathrm{GeV}^2/c^4$ and $q^2 > 14.4\,\mathrm{GeV}^2/c^4$ ranges. Although our results in the q^2_0 range are consistent with both the SM expectation as well as a possible suppression in the decay rate, our results in the q^2_5 range show an excess, rather than a deficit, of $\sim 2\sigma$ in both the $B \to X_s\, e^+e^-$ and $B \to X_s\, \mu^+\mu^-$ rates with respect to the SM expectation [22].

We search for CP violation in each q^2 bin by dividing our dataset into four disjoint samples according to lepton identity (e^+e^- or $\mu^+\mu^-$) and the B or $\overline{B}$ flavor as determined by the kaon and pion charges of the X_s system. Modes with $X_s = K^0_S$, $K^0_S\pi^0$ or $K^0_S\pi^+\pi^-$ are not used; and, because we perform no model-dependent extrapolation of signal rates, we measure A_{CP} only for the particular combination of final states used here. We simultaneously fit all four datasets, sharing a single value of A_{CP} as a free parameter, using the BFs fit model described above. Our A_{CP} results are shown in Table I; a plot of the results as a function of q^2 is included as part of our supplemental EPAPS material [56]. We analyze the vetoed J/ψ dataset, where CP violation is ex-

pected to be trivially small [69, 70], with the same fitting methodology used for the signal q^2 bins; we find $A_{CP}^{\bar{c}cs} = 0.0046 \pm 0.0057$[stat]. Observing no significant bias, we assign the statistical uncertainty here as the systematic uncertainty for the A_{CP} results. To extract A_{CP} for the full dilepton mass range, we sum the A_{CP} BFs across the four disjoint A_{CP} q^2 bins; excluding the charmonium veto windows, we find $A_{CP} = 0.04 \pm 0.11$[stat]± 0.01[syst]. We observe no significant asymmetry in any q^2 region or for the full dilepton mass range.

In summary, we have measured the total and partial BFs, as well as A_{CP}, for the inclusive radiative electroweak process $B \to X_s\,\ell^+\ell^-$. Our results are in general agreement with SM expectations with the exception of our partial BF results in the high-q^2 region, which show a $\sim 2\sigma$ excess compared to both the SM expectation and the most favored value of the beyond-SM contribution $C_9^{\rm BSM}$ advanced to explain recent observations by LHCb [35].

We are grateful to Enrico Lunghi, Tobias Hurth and Tobias Huber for useful discussions, as well as providing dilepton mass-squared theory distributions derived using the most up-to-date corrections. We are additionally grateful for the excellent luminosity and machine conditions provided by our PEP-II colleagues, and for the substantial dedicated effort from the computing organizations that support *BABAR*. The collaborating institutions wish to thank SLAC for its support and kind hospitality. This work is supported by DOE and NSF (USA), NSERC (Canada), CEA and CNRS-IN2P3 (France), BMBF and DFG (Germany), INFN (Italy), FOM (The Netherlands), NFR (Norway), MES (Russia), MINECO (Spain), STFC (United Kingdom). Individuals have received support from the Marie Curie EIF (European Union) and the A. P. Sloan Foundation (USA).

* Now at the University of Tabuk, Tabuk 71491, Saudi Arabia
† Also with Università di Perugia, Dipartimento di Fisica, Perugia, Italy
‡ Now at Laboratoire de Physique Nucléaire et de Hautes Energies, IN2P3/CNRS, Paris, France
§ Now at the University of Huddersfield, Huddersfield HD1 3DH, UK
¶ Deceased
** Now at University of South Alabama, Mobile, Alabama 36688, USA
†† Also with Università di Sassari, Sassari, Italy
‡‡ Also with INFN Sezione di Roma, Roma, Italy
§§ Now at Universidad Técnica Federico Santa Maria, Valparaiso, Chile 2390123

[1] G. Buchalla, A. J. Buras, and M. E. Lautenbacher, Rev. Mod. Phys. **68**, 1125 (1996).
[2] W. Altmannshofer, P. Paradisi, and D. M. Straub, JHEP **1204**, 008 (2012).
[3] N. Kosnik, Phys. Rev. D **86**, 055004 (2012).
[4] J. Drobnak, S. Fajfer, and J. F. Kamenik, Nucl. Phys. B **855**, 82 (2012).
[5] S. Descotes-Genon, D. Ghosh, J. Matias, and M. Ramon, JHEP **1106**, 099 (2011).
[6] S. Oh and J. Tandean, Phys. Rev. D **83**, 095006 (2011).
[7] K. S. M. Lee, and F. J. Tackmann, Phys. Rev. D **79**, 114021 (2009).
[8] A. Ali, E. Lunghi, C. Greub, and G. Hiller, Phys. Rev. D **66**, 034002 (2002).
[9] P. Gambino, U. Haisch, and M. Misiak, Phys. Rev. Lett. **94**, 061803 (2005).
[10] A. K. Alok, A. Dighe and S. Ray, Phys. Rev. D **79**, 034017 (2009).
[11] A. Soni, A. K. Alok, A. Giri, R. Mohanta and S. Nandi, Phys. Rev. D **82**, 033009 (2010).
[12] J. Beringer *et al.* [Particle Data Group Collaboration], Phys. Rev. D **86**, 010001 (2012).
[13] H. H. Asatryan, H. M. Asatrian, C. Greub, and M. Walker, Phys. Rev. D **65**, 074004 (2002).
[14] H. H. Asatryan, H. M. Asatrian, C. Greub, and M. Walker, Phys. Rev. D **66**, 034009 (2002).
[15] A. Ghinculov, T. Hurth, G. Isidori, and Y. P. Yao, Nucl. Phys. B **648**, 254 (2003).
[16] H. M. Asatrian, K. Bieri, C. Greub, and A. Hovhannisyan, Phys. Rev. D **66**, 094013 (2002).
[17] P. Gambino, M. Gorbahn, and U. Haisch, Nucl. Phys. B **673**, 238 (2003).
[18] A. Ghinculov, T. Hurth, G. Isidori, and Y. P. Yao, Eur. Phys. J. C **33**, S288 (2004).
[19] C. Bobeth, P. Gambino, M. Gorbahn, and U. Haisch, JHEP **0404**, 071 (2004).
[20] A. Ghinculov, T. Hurth, G. Isidori, and Y. P. Yao, Nucl. Phys. B **685**, 351 (2004).
[21] C. Greub, V. Pilipp, and C. Schupbach, JHEP **0812**, 040 (2008).
[22] T. Huber, T. Hurth, and E. Lunghi, Nucl. Phys. B **802**, 40 (2008).
[23] T. Huber, E. Lunghi, M. Misiak, and D. Wyler, Nucl. Phys. B **740**, 105 (2006).
[24] M. Beneke, G. Buchalla, M. Neubert, and C. T. Sachrajda, Eur. Phys. J. C **61**, 439 (2009).
[25] D.S. Du and M.Z. Yang, Phys. Rev. D **54**, 882 (1996).
[26] A. Ali and G. Hiller, Eur. Phys. J. C **8**, 619 (1999).
[27] C. Bobeth, G. Hiller and G. Piranishvili, JHEP **0807**, 106 (2008).
[28] W. Altmannshofer *et al.*, JHEP **0901**, 019 (2009).
[29] B. Aubert *et al.* [*BABAR* Collaboration], Phys. Rev. Lett. **93**, 081802 (2004).
[30] M. Iwasaki *et al.* [Belle Collaboration], Phys. Rev. D **72**, 092005 (2005).
[31] J. P. Lees *et al.* [*BABAR* Collaboration], Phys. Rev. D **86**, 032012 (2012).
[32] J. -T. Wei *et al.* [Belle Collaboration], Phys. Rev. Lett. **103**, 171801 (2009).
[33] T. Aaltonen *et al.* [CDF Collaboration], Phys. Rev. Lett. **107**, 201802 (2011).
[34] R. Aaij *et al.* [LHCb Collaboration], Phys. Rev. Lett. **108**, 181806 (2012).
[35] R. Aaij *et al.* [LHCb Collaboration], Phys. Rev. Lett. **111**, 191801 (2013).
[36] B. Aubert *et al.* [*BABAR* Collaboration], Phys. Rev. D **79**, 031102 (2009).
[37] R. Aaij *et al.* [LHCb Collaboration], Phys. Rev. Lett.

110, 031801 (2013).
[38] J. P. Lees *et al.* [*BABAR* Collaboration], Nucl. Instrum. Meth. A **726**, 203 (2013).
[39] B. Aubert *et al.* [*BABAR* Collaboration], Nucl. Instrum. Meth. A **479**, 1 (2002).
[40] B. Aubert *et al.* [*BABAR* Collaboration], Nucl. Instrum. Meth. A **729**, 615 (2013).
[41] The use of charge conjugate reactions is implied unless otherwise indicated.
[42] F. Kruger and L. M. Sehgal, Phys. Lett. B **380**, 199 (1996).
[43] A. Ali, G. Hiller, L. T. Handoko, and T. Morozumi, Phys. Rev. D **55**, 4105 (1997).
[44] C. Bobeth, M. Misiak, and J. Urban, Nucl. Phys. B **574**, 291 (2000).
[45] T. Sjöstrand, Comput. Phys. Commun. **82**, 74 (1994).
[46] P. Ball and R. Zwicky, Phys. Rev. D **71**, 014029 (2005).
[47] P. Ball and R. Zwicky, Phys. Rev. D **71**, 014015 (2005).
[48] L. Breiman, Mach. Learn. **24**, 123 (1996).
[49] I. Narsky, arXiv:physics/0507157 (2005).
[50] M. J. Oreglia, Ph.D. Thesis, SLAC-236 (1980).
[51] J. E. Gaiser, Ph.D. Thesis, SLAC-255 (1982).
[52] T. Skwarnicki, DESY-F31-86-02.
[53] E. Parzen, Ann. Math. Statist. Vol. 33 **3**, 1065 (1962).
[54] V.A. Epanechnikov, Theory Probab. Appl. **14**, 153 (1962).
[55] B. Aubert *et al.* [*BABAR* Collaboration], Phys. Rev. D **73**, 092001 (2006).
[56] A URL OR OTHER METHOD FOR ACCESSING THE SUPPLEMENTAL MATERIAL WILL BE PROVIDED BY APS EDITORIAL STAFF. THE LINK/INFO WILL BE HERE.
[57] Y. Amhis *et al.* [Heavy Flavor Averaging Group Collaboration], arXiv:1207.1158 [hep-ex], updated Aug. 2012.
[58] B. Aubert *et al.* [*BABAR* Collaboration], Phys. Rev. D **69**, 071101 (2004).
[59] S. Descotes-Genon, J. Matias and J. Virto, Phys. Rev. D **88**, 074002 (2013).
[60] S. Jger and J. Martin Camalich, JHEP **1305**, 043 (2013).
[61] A. J. Buras and J. Girrbach, JHEP **1312**, 009 (2013).
[62] W. Altmannshofer and D. M. Straub, Eur. Phys. Jour. C **73**, 2646 (2013).
[63] R. Gauld, F. Goertz and U. Haisch, arXiv:1308.1959 [hep-ph].
[64] R. Gauld, F. Goertz and U. Haisch, arXiv:1310.1082 [hep-ph].
[65] F. Beaujean, C. Bobeth and D. van Dyk, arXiv:1310.2478 [hep-ph].
[66] R. R. Horgan, Z. Liu, S. Meinel and M. Wingate, arXiv:1310.3887 [hep-ph].
[67] A. J. Buras, F. De Fazio and J. Girrbach, arXiv:1311.6729 [hep-ph].
[68] T. Hurth and F. Mahmoudi, arXiv:1312.5267 [hep-ph].
[69] G. -H. Wu and A. Soni, Phys. Rev. D **62**, 056005 (2000).
[70] W. -S. Hou, M. Nagashima and A. Soddu, hep-ph/0605080.

Introduction

This Supplemental Material includes:

- Figure 2, plotting the A_{CP} results as a function of q^2;
- Figure 3, plotting the differential branching fraction as a function of m_{X_s};
- Table II, giving in each individual q^2 and m_{X_s} bin the fitted raw number of signal events $N_{\rm sig}$, as well as the fitted number of random combinatorial $B\overline{B}$ background events $N_{B\overline{B}}$ present in the signal enhanced region with $m_{\rm ES} > 5.27\,{\rm GeV}/c^2$;
- Tables III-VIII, detailing individual contributions to the "additive" and "multiplicative" branching fraction systematics (as defined in the article main text), and the model-dependent extrapolation systematics; and
- Figures 4-23, which show the projections of our branching fraction fits onto their respective datasets.

A_{CP} **results.**

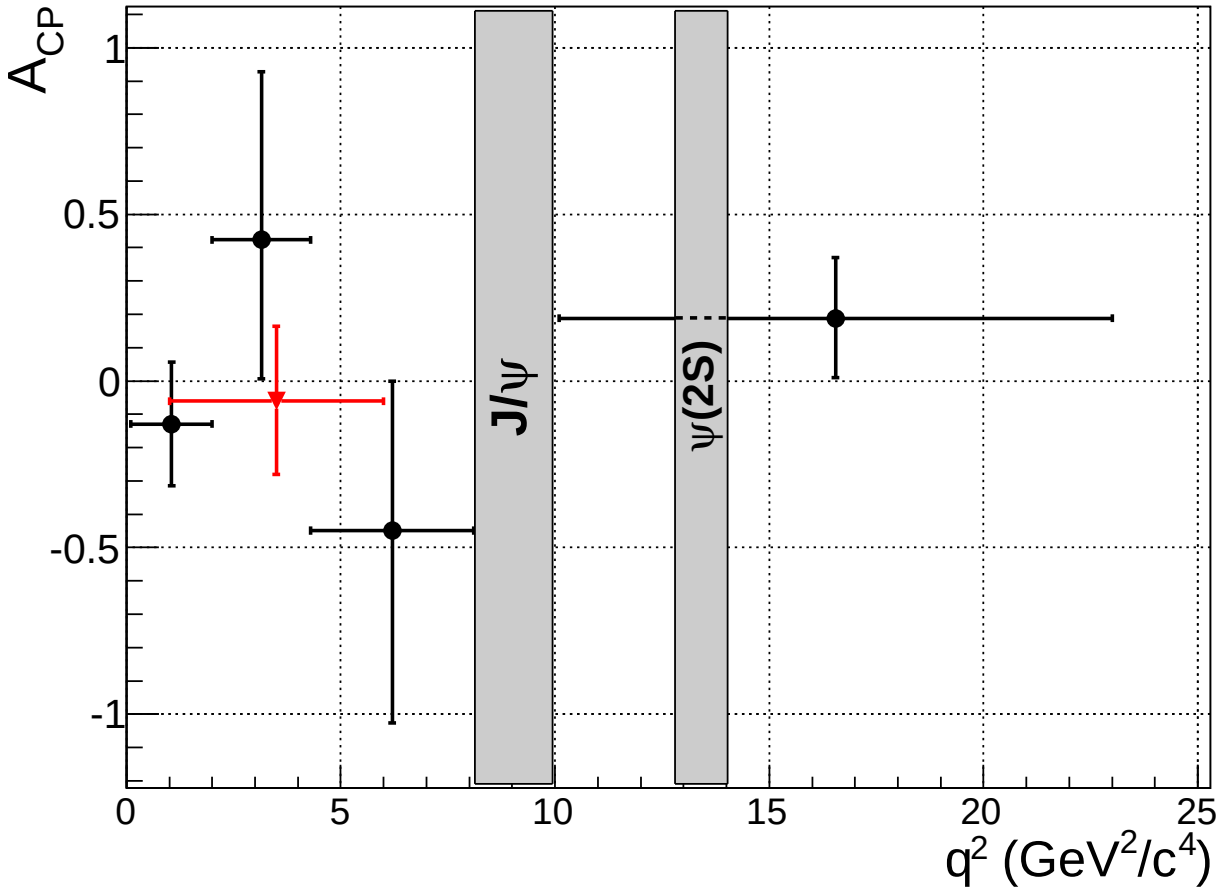

FIG. 2: Results for A_{CP} as a function of q^2. The black points show the $q^2_1 - q^2_{45}$ results; the red triangle denotes q^2_0. The q^2_{45} A_{CP} result does not include events in the $\psi(2S)$ veto window.

Differental Branching Fraction in m_{X_s} bins.

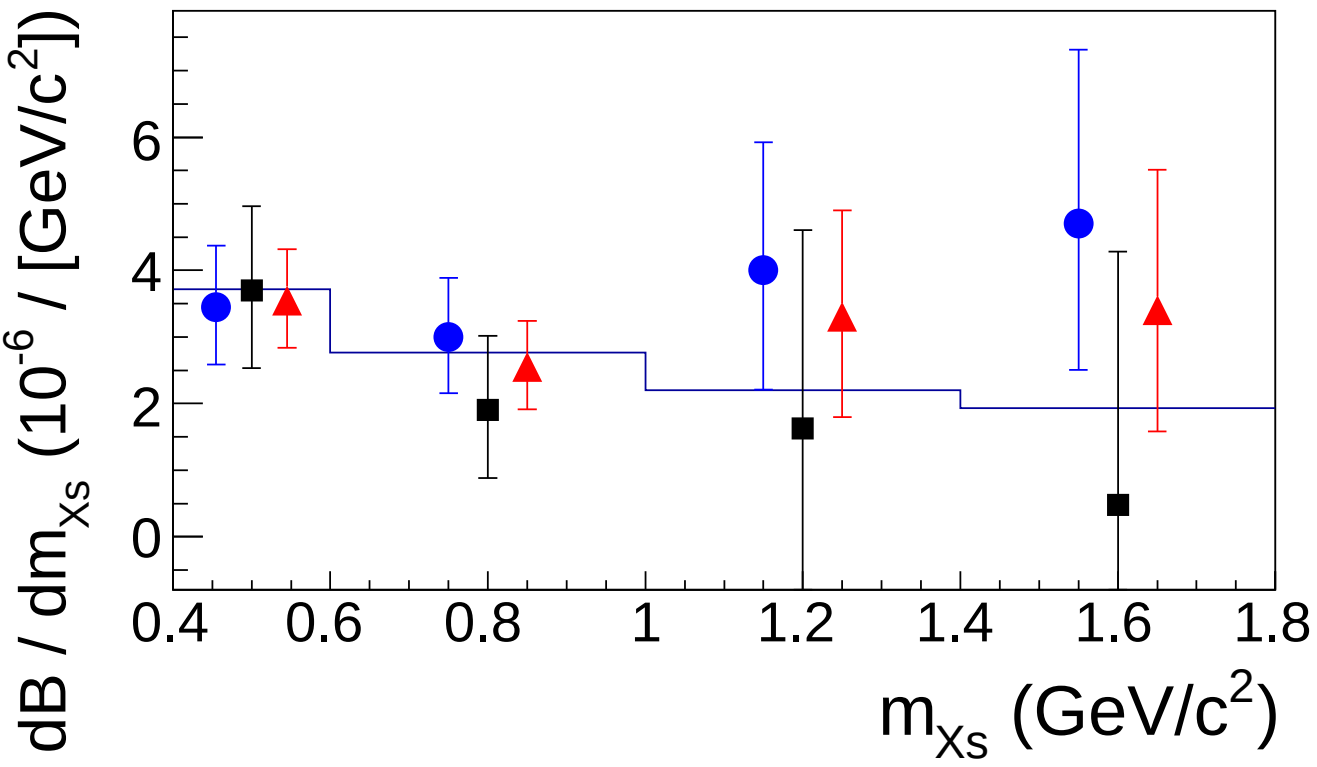

FIG. 3: Differential BF as a function of m_{X_s} for electron (blue circles), muon (black squares) and lepton-flavor-averaged final states (red triangles). The errors correspond to the total uncertainties. The histogram shows the SM expectation, which has uncertainties of approximately 10-30% as a function of q^2. Estimated contributions from the vetoed charmonium q^2 regions are included. The horizontal spread of points in each bin is meant only to aid visibility.

Fitted Signal and Background Yields

Table II gives the fitted number of signal events $N_{\rm sig}$ in each individual q^2 and m_{X_s} bin, along with the fitted number of random combinatorial $B\overline{B}$ background events $N_{B\overline{B}}$ present in the signal enhanced region with $m_{\rm ES} > 5.27\,{\rm GeV}/c^2$. The quoted uncertainties are statistical only.

TABLE II: Fitted number of signal events $N_{\rm sig}$ and random combinatorial $B\overline{B}$ background events $N_{B\overline{B}}$ present in the signal enhanced region with $m_{\rm ES} > 5.27\,{\rm GeV}/c^2$ by $q^2({\rm GeV}^2/c^4)$ and $m_{X_s}({\rm GeV}/c^2)$ bin.

		$B \to X_s\, e^+e^-$		$B \to X_s\, \mu^+\mu^-$	
Bin	Range	$N_{\rm sig}$	$N_{B\overline{B}}$	$N_{\rm sig}$	$N_{B\overline{B}}$
q^2_0	$1.0 < q^2 < 6.0$	$58.5^{+14.4}_{-13.5}$	348.8 ± 22.2	$8.6^{+11.2}_{-10.4}$	521.8 ± 29.5
q^2_1	$0.1 < q^2 < 2.0$	$60.4^{+11.9}_{-11.1}$	95.3 ± 12.4	$13.3^{+7.7}_{-6.9}$	28.4 ± 7.6
q^2_2	$2.0 < q^2 < 4.3$	$20.8^{+9.4}_{-8.5}$	168.2 ± 15.3	$-1.9^{+6.9}_{-5.8}$	50.5 ± 8.6
q^2_3	$4.3 < q^2 < 6.8$	$25.4^{+10.3}_{-9.5}$	181.3 ± 16.2	$6.0^{+9.0}_{-8.3}$	58.5 ± 10.2
q^2_4	$10.1 < q^2 < 12.9$	$59.1^{+14.8}_{-14.0}$	201.0 ± 20.3	$25.5^{+10.4}_{-9.6}$	107.6 ± 13.6
q^2_5	$14.2 < q^2$	$41.0^{+8.3}_{-7.7}$	40.2 ± 10.0	$23.3^{+7.3}_{-6.7}$	20.0 ± 8.5
$m_{X_s,1}$	$0.4 < m_{X_s} < 0.6$	$63.0^{+9.9}_{-9.2}$	3.0 ± 2.9	$34.0^{+6.8}_{-6.1}$	2.0 ± 1.9
$m_{X_s,2}$	$0.6 < m_{X_s} < 1.0$	$68.1^{+11.5}_{-10.9}$	38.0 ± 8.9	$22.0^{+7.3}_{-6.7}$	12.1 ± 6.2
$m_{X_s,3}$	$1.0 < m_{X_s} < 1.4$	$38.1^{+11.9}_{-11.3}$	168.1 ± 17.9	$7.3^{+9.0}_{-8.4}$	80.9 ± 12.3
$m_{X_s,4}$	$1.4 < m_{X_s} < 1.8$	$28.5^{+12.9}_{-12.3}$	483.9 ± 28.6	$1.3^{+10.3}_{-9.5}$	171.2 ± 17.5

Systematics Tables

Tables III-VIII detail the individual contributions to the branching fraction systematics. Uncertainties quoted without a preceding "+" or "−" are ± symmetric.

TABLE III: $B \to X_s\, e^+e^-$ branching fraction "multiplicative" systematic uncertainties.

Variation	q_0^2	q_1^2	q_2^2	q_3^2	q_4^2	q_5^2	$m_{X_s,1}$	$m_{X_s,2}$	$m_{X_s,3}$	$m_{X_s,4}$
$N_{B\overline{B}}$	0.012	0.018	0.004	0.004	0.007	0.003	0.004	0.007	0.010	0.011
Tracking efficiency	0.031	0.049	0.011	0.011	0.018	0.009	0.011	0.019	0.026	0.030
Particle Identification efficiency	0.033	0.052	0.012	0.012	0.019	0.010	0.012	0.020	0.027	0.032
K_S^0 efficiency	0.004	0.006	0.001	0.001	0.001	0.001	0.001	0.002	0.002	0.002
π^0 efficiency	0.012	0.024	0.004	0.004	0.006	0.002	0.000	0.008	0.014	0.019
BDT efficiency correction	0.004	0.006	0.001	0.001	0.009	0.004	0.001	0.002	0.003	0.004
Monte Carlo statistics	0.002	0.009	0.002	0.002	0.003	0.001	0.001	0.001	0.002	0.006
Total	0.048	0.079	0.017	0.017	0.030	0.014	0.017	0.030	0.041	0.050

TABLE IV: $B \to X_s\, \mu^+\mu^-$ branching fraction "multiplicative" systematic uncertainties.

Variation	q_0^2	q_1^2	q_2^2	q_3^2	q_4^2	q_5^2	$m_{X_s,1}$	$m_{X_s,2}$	$m_{X_s,3}$	$m_{X_s,4}$
$N_{B\overline{B}}$	0.004	0.011	0.001	0.002	0.005	0.004	0.004	0.005	0.004	0.001
Tracking efficiency	0.009	0.027	0.002	0.005	0.011	0.007	0.008	0.011	0.010	0.003
Particle Identification efficiency	0.015	0.042	0.003	0.008	0.020	0.014	0.017	0.017	0.015	0.004
K_S^0 efficiency	0.001	0.004	0.000	0.001	0.002	0.001	0.001	0.002	0.001	0.000
π^0 efficiency	0.004	0.013	0.001	0.002	0.004	0.002	0.000	0.005	0.005	0.002
BDT efficiency correction	0.002	0.005	0.000	0.001	0.010	0.007	0.002	0.002	0.002	0.001
Monte Carlo statistics	0.001	0.005	0.000	0.001	0.003	0.001	0.001	0.001	0.001	0.001
Total	0.019	0.054	0.004	0.010	0.026	0.018	0.020	0.022	0.019	0.006

TABLE V: $B \to X_s\, e^+e^-$ branching fraction "additive" systematic uncertainties.

Variation	q_0^2	q_1^2	q_2^2	q_3^2	q_4^2	q_5^2	$m_{X_s,1}$	$m_{X_s,2}$	$m_{X_s,3}$	$m_{X_s,4}$
Signal $m_{\rm ES}$ pdf shape	$^{+0.039}_{-0.019}$	$^{+0.092}_{-0.092}$	$^{+0.007}_{-0.014}$	$^{+0.014}_{-0.008}$	$^{+0.034}_{-0.034}$	$^{+0.011}_{-0.005}$	$^{+0.021}_{-0.007}$	$^{+0.036}_{-0.012}$	$^{+0.032}_{-0.017}$	$^{+0.057}_{-0.057}$
Signal L_R pdf shape	$^{+0.077}_{-0.026}$	$^{+0.159}_{-0.000}$	$^{+0.055}_{-0.012}$	$^{+0.006}_{-0.000}$	$^{+0.142}_{-0.000}$	$^{+0.002}_{-0.001}$	$^{+0.002}_{-0.001}$	$^{+0.050}_{-0.000}$	$^{+0.127}_{-0.000}$	$^{+0.474}_{-0.000}$
Crossfeed pdf shape	$^{+0.032}_{-0.014}$	$^{+0.074}_{-0.090}$	$^{+0.026}_{-0.009}$	$^{+0.015}_{-0.003}$	$^{+0.067}_{-0.016}$	$^{+0.000}_{-0.015}$	$^{+0.002}_{-0.001}$	$^{+0.013}_{-0.000}$	$^{+0.055}_{-0.017}$	$^{+0.201}_{-0.000}$
Crossfeed normalization	$^{+0.034}_{-0.026}$	$^{+0.039}_{-0.022}$	$^{+0.014}_{-0.014}$	$^{+0.011}_{-0.009}$	$^{+0.021}_{-0.019}$	$^{+0.008}_{-0.008}$	$^{+0.002}_{-0.001}$	$^{+0.014}_{-0.013}$	$^{+0.027}_{-0.033}$	$^{+0.011}_{-0.025}$
$B\overline{B}$ pdf shape	$^{+0.159}_{-0.123}$	$^{+0.139}_{-0.096}$	$^{+0.080}_{-0.052}$	$^{+0.086}_{-0.070}$	$^{+0.010}_{-0.038}$	$^{+0.014}_{-0.000}$	$^{+0.006}_{-0.005}$	$^{+0.020}_{-0.019}$	$^{+0.126}_{-0.099}$	$^{+0.367}_{-0.351}$
udsc pdf shape	$^{+0.063}_{-0.050}$	$^{+0.106}_{-0.094}$	$^{+0.026}_{-0.021}$	$^{+0.032}_{-0.034}$	$^{+0.035}_{-0.026}$	$^{+0.014}_{-0.012}$	$^{+0.005}_{-0.006}$	$^{+0.021}_{-0.025}$	$^{+0.087}_{-0.089}$	$^{+0.181}_{-0.231}$
udsc normalization	$^{+0.019}_{-0.007}$	$^{+0.059}_{-0.039}$	$^{+0.009}_{-0.005}$	$^{+0.011}_{-0.006}$	$^{+0.019}_{-0.009}$	$^{+0.008}_{-0.003}$	$^{+0.003}_{-0.003}$	$^{+0.010}_{-0.013}$	$^{+0.030}_{-0.031}$	$^{+0.055}_{-0.057}$
Charmonium pdf shape	$^{+0.055}_{-0.029}$	$^{+0.020}_{-0.006}$	$^{+0.019}_{-0.012}$	$^{+0.032}_{-0.046}$	$^{+0.115}_{-0.038}$	$^{+0.005}_{-0.000}$	$^{+0.006}_{-0.000}$	$^{+0.034}_{-0.018}$	$^{+0.126}_{-0.061}$	$^{+0.231}_{-0.139}$
Charmonium normalization	$^{+0.041}_{-0.034}$	$^{+0.022}_{-0.006}$	$^{+0.024}_{-0.021}$	$^{+0.041}_{-0.037}$	$^{+0.075}_{-0.067}$	$^{+0.012}_{-0.007}$	$^{+0.025}_{-0.024}$	$^{+0.046}_{-0.048}$	$^{+0.093}_{-0.097}$	$^{+0.107}_{-0.113}$
Total	$^{+0.210}_{-0.147}$	$^{+0.275}_{-0.192}$	$^{+0.110}_{-0.066}$	$^{+0.109}_{-0.099}$	$^{+0.216}_{-0.100}$	$^{+0.029}_{-0.023}$	$^{+0.034}_{-0.026}$	$^{+0.092}_{-0.064}$	$^{+0.265}_{-0.183}$	$^{+0.709}_{-0.465}$

TABLE VI: $B \to X_s\,\mu^+\mu^-$ branching fraction "additive" systematic uncertainties.

Variation	q_0^2	q_1^2	q_2^2	q_3^2	q_4^2	q_5^2	$m_{X_s,1}$	$m_{X_s,2}$	$m_{X_s,3}$	$m_{X_s,4}$
Signal $m_{\rm ES}$ pdf shape	$^{+0.012}_{-0.007}$	$^{+0.055}_{-0.018}$	$^{+0.004}_{-0.004}$	$^{+0.010}_{-0.006}$	$^{+0.008}_{-0.008}$	$^{+0.012}_{-0.012}$	$^{+0.022}_{-0.022}$	$^{+0.008}_{-0.015}$	$^{+0.019}_{-0.019}$	$^{+0.006}_{-0.004}$
Signal L_R pdf shape	$^{+0.030}_{-0.048}$	$^{+0.000}_{-0.069}$	$^{+0.029}_{-0.038}$	$^{+0.000}_{-0.025}$	$^{+0.024}_{-0.001}$	$^{+0.003}_{-0.002}$	$^{+0.000}_{-0.003}$	$^{+0.000}_{-0.008}$	$^{+0.000}_{-0.098}$	$^{+0.378}_{-0.000}$
Crossfeed pdf shape	$^{+0.018}_{-0.020}$	$^{+0.077}_{-0.123}$	$^{+0.029}_{-0.011}$	$^{+0.010}_{-0.006}$	$^{+0.039}_{-0.035}$	$^{+0.018}_{-0.015}$	$^{+0.003}_{-0.003}$	$^{+0.033}_{-0.006}$	$^{+0.077}_{-0.026}$	$^{+0.136}_{-0.118}$
Crossfeed normalization	$^{+0.025}_{-0.020}$	$^{+0.030}_{-0.008}$	$^{+0.005}_{-0.002}$	$^{+0.016}_{-0.013}$	$^{+0.020}_{-0.017}$	$^{+0.007}_{-0.006}$	$^{+0.002}_{-0.001}$	$^{+0.007}_{-0.007}$	$^{+0.017}_{-0.039}$	$^{+0.017}_{-0.011}$
$B\overline{B}$ pdf shape	$^{+0.226}_{-0.121}$	$^{+0.141}_{-0.063}$	$^{+0.094}_{-0.045}$	$^{+0.097}_{-0.054}$	$^{+0.058}_{-0.009}$	$^{+0.011}_{-0.000}$	$^{+0.002}_{-0.005}$	$^{+0.012}_{-0.013}$	$^{+0.182}_{-0.104}$	$^{+0.340}_{-0.199}$
$udsc$ pdf shape	$^{+0.050}_{-0.050}$	$^{+0.083}_{-0.065}$	$^{+0.013}_{-0.007}$	$^{+0.065}_{-0.078}$	$^{+0.024}_{-0.021}$	$^{+0.013}_{-0.012}$	$^{+0.001}_{-0.000}$	$^{+0.033}_{-0.029}$	$^{+0.064}_{-0.070}$	$^{+0.117}_{-0.136}$
$udsc$ normalization	$^{+0.030}_{-0.016}$	$^{+0.059}_{-0.042}$	$^{+0.207}_{-0.000}$	$^{+0.022}_{-0.016}$	$^{+0.021}_{-0.015}$	$^{+0.003}_{-0.000}$	$^{+0.005}_{-0.004}$	$^{+0.012}_{-0.013}$	$^{+0.032}_{-0.040}$	$^{+0.069}_{-0.065}$
Charmonium pdf shape	$^{+0.069}_{-0.121}$	$^{+0.030}_{-0.030}$	$^{+0.032}_{-0.056}$	$^{+0.056}_{-0.033}$	$^{+0.019}_{-0.022}$	$^{+0.003}_{-0.000}$	$^{+0.002}_{-0.001}$	$^{+0.024}_{-0.007}$	$^{+0.026}_{-0.066}$	$^{+0.306}_{-0.283}$
Charmonium normalization	$^{+0.134}_{-0.117}$	$^{+0.083}_{-0.073}$	$^{+0.085}_{-0.081}$	$^{+0.102}_{-0.095}$	$^{+0.039}_{-0.032}$	$^{+0.004}_{-0.000}$	$^{+0.007}_{-0.007}$	$^{+0.032}_{-0.033}$	$^{+0.098}_{-0.106}$	$^{+0.246}_{-0.231}$
Hadronic misidentification pdf shape	$^{+0.098}_{-0.087}$	$^{+0.099}_{-0.085}$	$^{+0.061}_{-0.063}$	$^{+0.060}_{-0.054}$	$^{+0.051}_{-0.044}$	$^{+0.030}_{-0.026}$	$^{+0.029}_{-0.028}$	$^{+0.034}_{-0.035}$	$^{+0.099}_{-0.109}$	$^{+0.195}_{-0.187}$
Hadronic misidentification normalization	$^{+0.030}_{-0.027}$	$^{+0.166}_{-0.111}$	$^{+0.049}_{-0.038}$	$^{+0.059}_{-0.021}$	$^{+0.012}_{-0.021}$	$^{+0.007}_{-0.012}$	$^{+0.012}_{-0.003}$	$^{+0.021}_{-0.022}$	$^{+0.084}_{-0.071}$	$^{+0.017}_{-0.078}$
Total	$^{+0.299}_{-0.239}$	$^{+0.292}_{-0.237}$	$^{+0.260}_{-0.137}$	$^{+0.187}_{-0.154}$	$^{+0.107}_{-0.079}$	$^{+0.043}_{-0.037}$	$^{+0.040}_{-0.037}$	$^{+0.076}_{-0.066}$	$^{+0.268}_{-0.249}$	$^{+0.699}_{-0.501}$

TABLE VII: $B \to X_s\,e^+e^-$ branching fraction model-dependent extrapolation systematic uncertainties.

Variation	q_0^2	q_1^2	q_2^2	q_3^2	q_4^2	q_5^2	$m_{X_s,3}$	$m_{X_s,4}$
Jetset tunings	$^{+0.060}_{-0.059}$	$^{+0.011}_{-0.013}$	$^{+0.010}_{-0.012}$	$^{+0.011}_{-0.014}$	$^{+0.001}_{-0.002}$	$^{+0.031}_{-0.036}$	$^{+0.037}_{-0.036}$	$^{+0.075}_{-0.077}$
$\pm 50\%$ $N_{\pi^0} > 1$	0.249	0.047	0.038	0.025	0.002	0.130	0.030	0.051
$\pm 50\%$ K multiplicity	0.046	0.008	0.006	0.002	0.000	0.022	0.000	0.006
$\pm 50\%$ π^+ multiplicity	0.196	0.036	0.028	0.012	0.000	0.100	0.024	0.080
$\pm 1\sigma$ $B \to K^{(*)}\ell^+\ell^-$ BFs	$^{+0.115}_{-0.129}$	$^{+0.024}_{-0.026}$	$^{+0.021}_{-0.023}$	$^{+0.018}_{-0.018}$	$^{+0.002}_{-0.002}$	$^{+0.067}_{-0.073}$	$^{+0.004}_{-0.005}$	$^{+0.000}_{-0.000}$
Total	$^{+0.346}_{-0.351}$	$^{+0.065}_{-0.066}$	$^{+0.053}_{-0.054}$	$^{+0.035}_{-0.036}$	$^{+0.003}_{-0.003}$	$^{+0.181}_{-0.184}$	$^{+0.053}_{-0.053}$	$^{+0.121}_{-0.123}$

TABLE VIII: $B \to X_s\,\mu^+\mu^-$ branching fraction model-dependent extrapolation systematic uncertainties.

Variation	q_0^2	q_1^2	q_2^2	q_3^2	q_4^2	q_5^2	$m_{X_s,3}$	$m_{X_s,4}$
Jetset tunings	$^{+0.035}_{-0.041}$	$^{+0.002}_{-0.003}$	$^{+0.005}_{-0.006}$	$^{+0.009}_{-0.012}$	$^{+0.001}_{-0.002}$	$^{+0.025}_{-0.020}$	$^{+0.015}_{-0.014}$	$^{+0.007}_{-0.008}$
$\pm 50\%$ $N_{\pi^0} > 1$	0.154	0.011	0.020	0.021	0.002	0.047	0.012	0.005
$\pm 50\%$ K multiplicity	0.029	0.002	0.003	0.002	0.000	0.008	0.000	0.001
$\pm 50\%$ π^+ multiplicity	0.122	0.008	0.015	0.010	0.000	0.036	0.010	0.008
$\pm 1\sigma$ $B \to K^{(*)}\ell^+\ell^-$ BFs	$^{+0.027}_{-0.030}$	$^{+0.002}_{-0.002}$	$^{+0.004}_{-0.005}$	$^{+0.007}_{-0.007}$	$^{+0.001}_{-0.001}$	$^{+0.015}_{-0.019}$	$^{+0.001}_{-0.001}$	$^{+0.000}_{-0.000}$
Total	$^{+0.203}_{-0.205}$	$^{+0.014}_{-0.014}$	$^{+0.026}_{-0.026}$	$^{+0.026}_{-0.027}$	$^{+0.003}_{-0.003}$	$^{+0.066}_{-0.065}$	$^{+0.021}_{-0.021}$	$^{+0.012}_{-0.013}$

Fit Projections

The pages following show the $B \to X_s\,e^+e^-$ and $B \to X_s\,\mu^+\mu^-$ branching fraction fit projections for each q^2 and m_{X_s} bin.

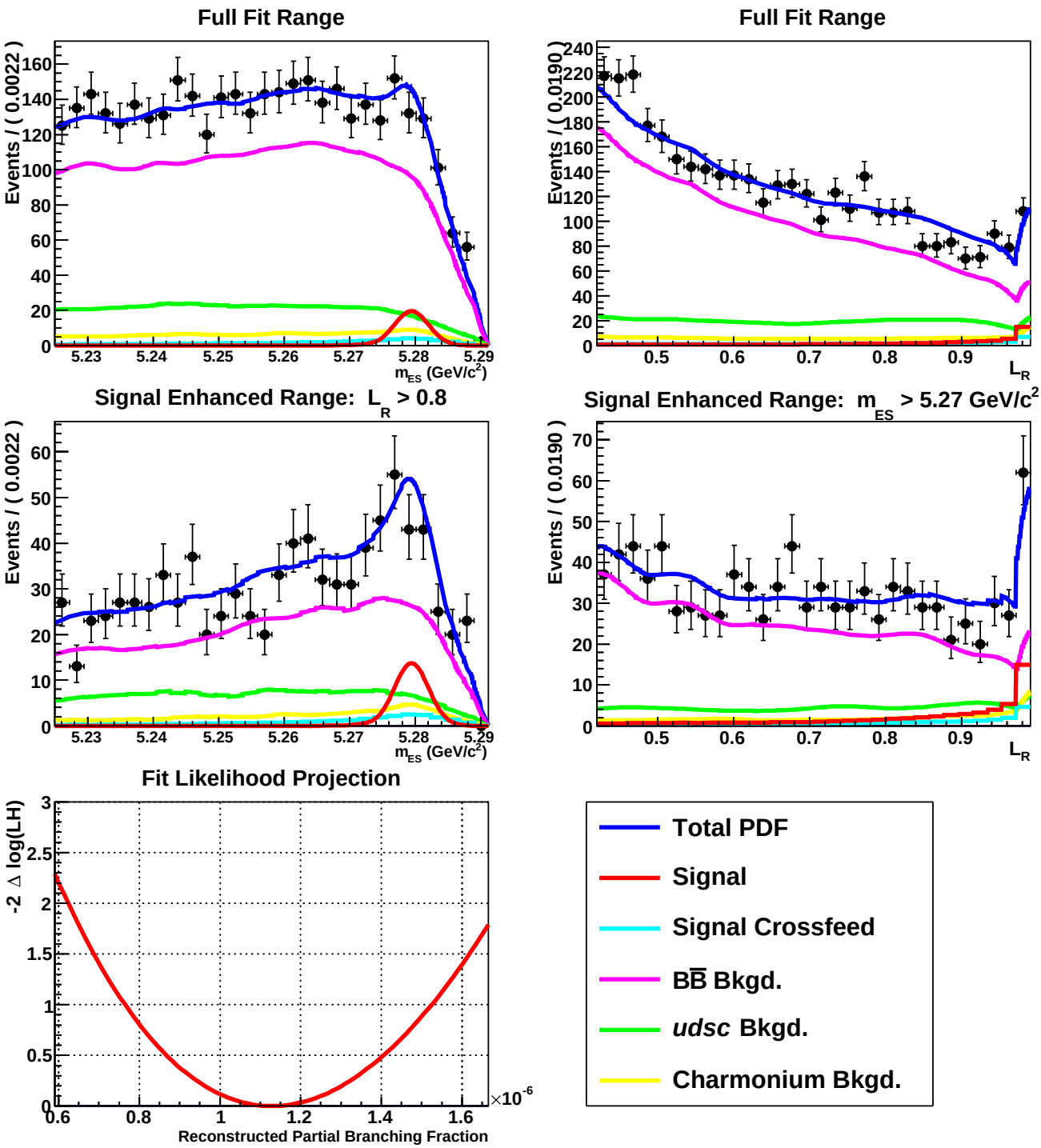

FIG. 4: Fit to $B \to X_s\, e^+ e^-$ in the q_0^2 bin. Top row left is the $m_{\rm ES}$ fit projection, top row right is the L_R fit projection; middle row left is a signal-enhanced $m_{\rm ES}$ fit projection for events with $L_R > 0.8$, middle row right is a signal-enhanced L_R fit projection for events in the $m_{\rm ES} > 5.27\,{\rm GeV}/c^2$ signal region. The lower left hand plot is the profile likelihood curve for the 2D data fit.

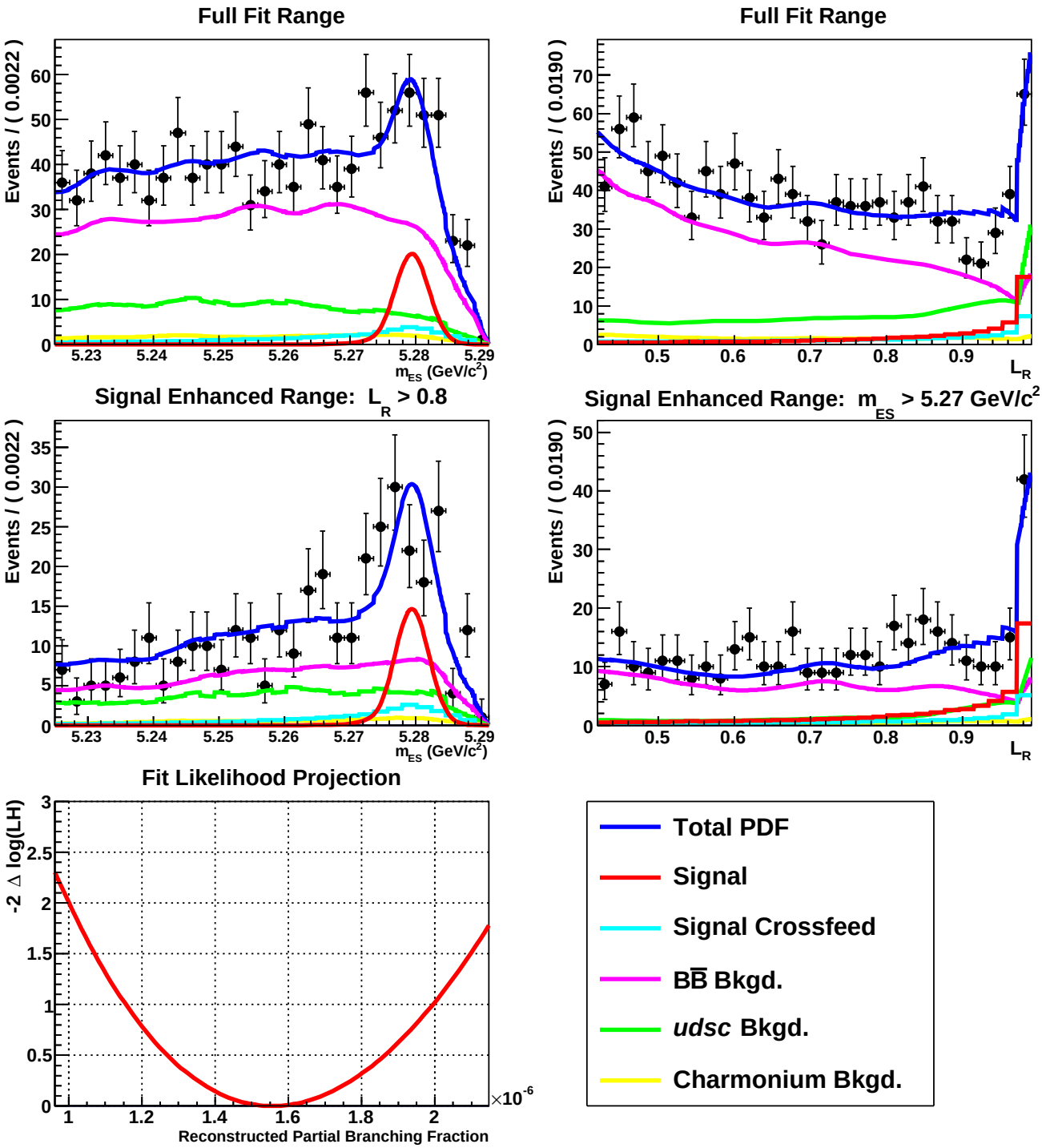

FIG. 5: Fit to $B \to X_s\, e^+ e^-$ in the q_1^2 bin. Top row left is the $m_{\rm ES}$ fit projection, top row right is the L_R fit projection; middle row left is a signal-enhanced $m_{\rm ES}$ fit projection for events with $L_R > 0.8$, middle row right is a signal-enhanced L_R fit projection for events in the $m_{\rm ES} > 5.27\,{\rm GeV}/c^2$ signal region. The lower left hand plot is the profile likelihood curve for the 2D data fit.

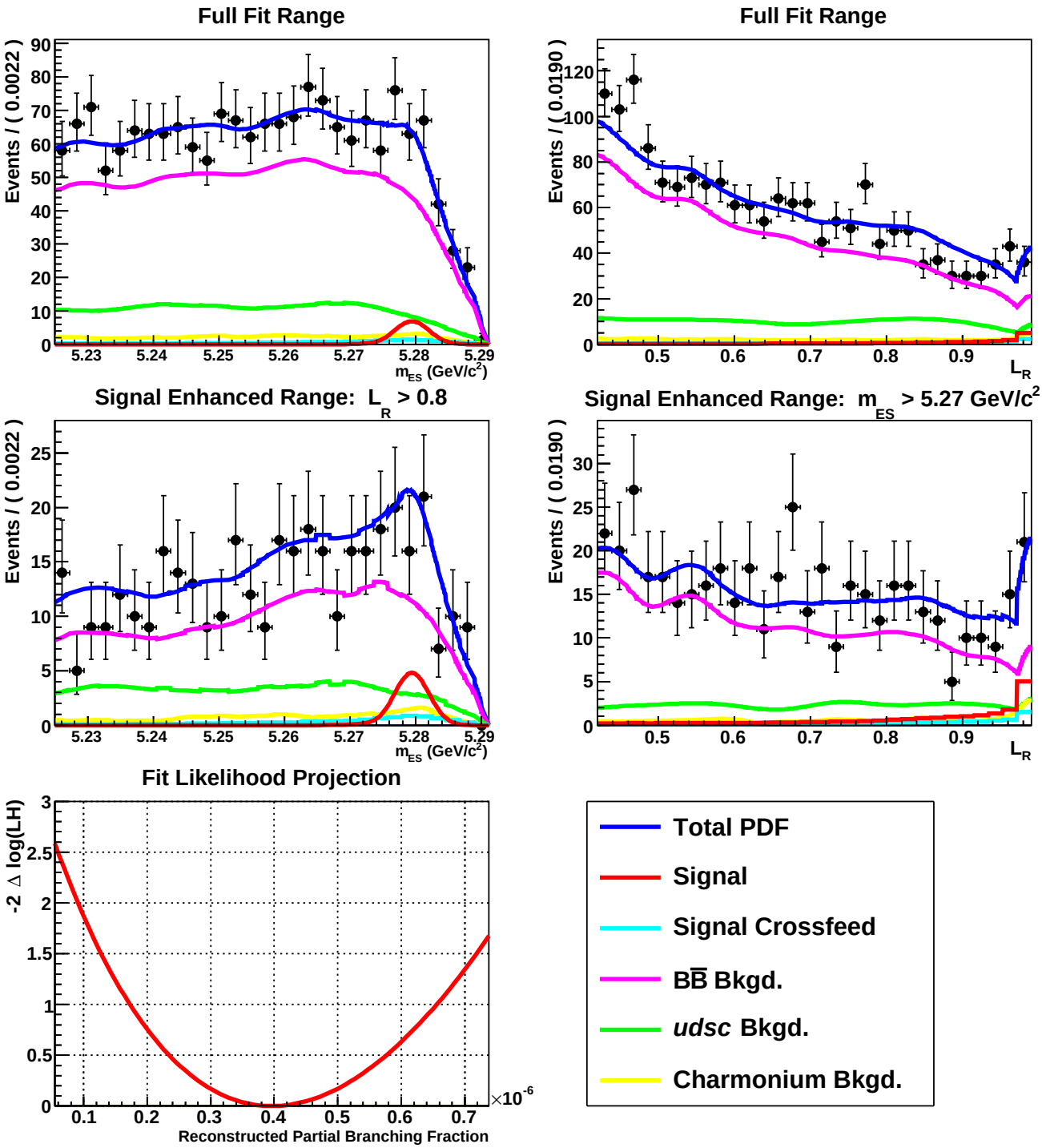

FIG. 6: Fit to $B \to X_s\, e^+ e^-$ in the q_2^2 bin. Top row left is the $m_{\rm ES}$ fit projection, top row right is the L_R fit projection; middle row left is a signal-enhanced $m_{\rm ES}$ fit projection for events with $L_R > 0.8$, middle row right is a signal-enhanced L_R fit projection for events in the $m_{\rm ES} > 5.27\,{\rm GeV}/c^2$ signal region. The lower left hand plot is the profile likelihood curve for the 2D data fit.

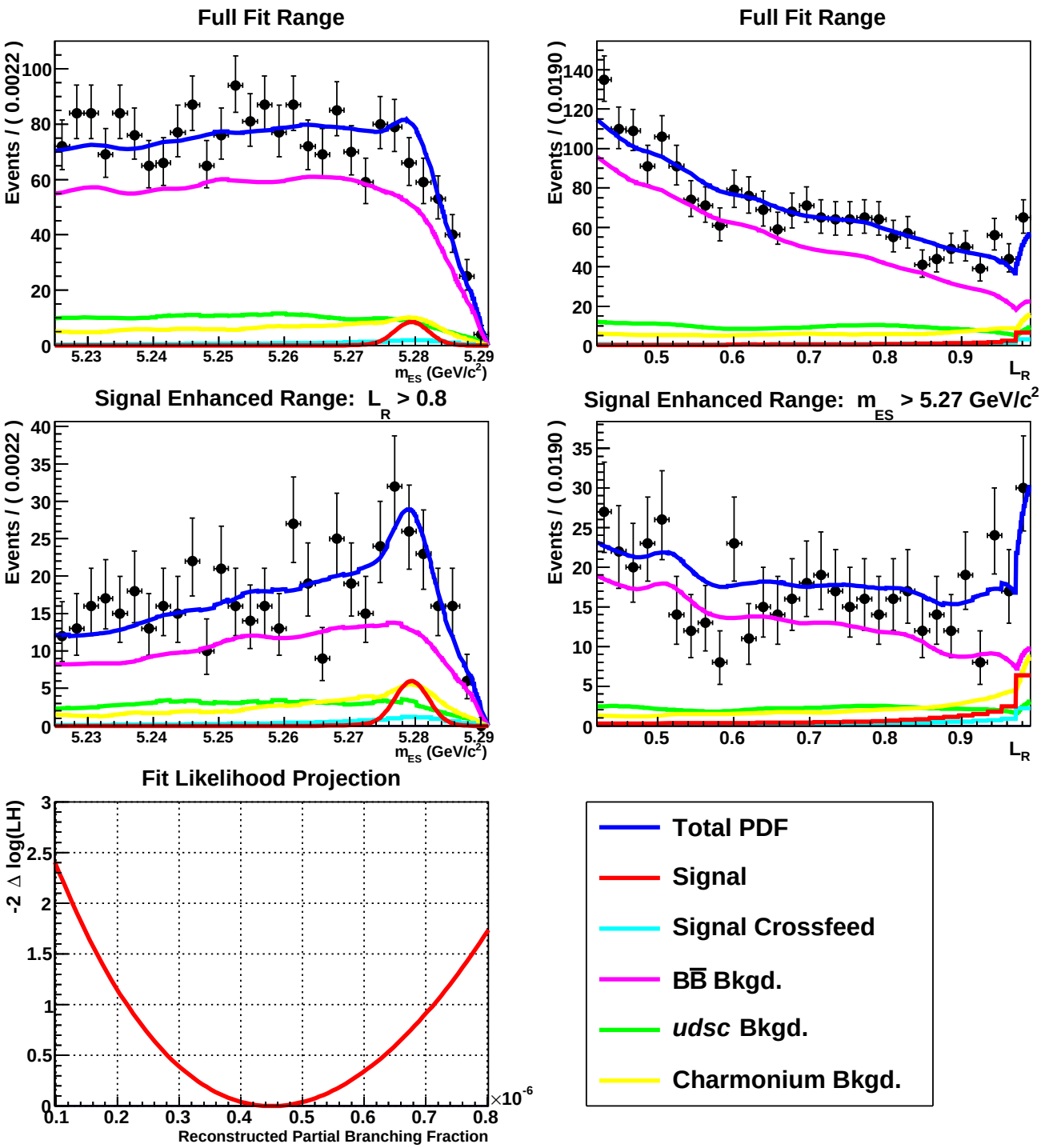

FIG. 7: Fit to $B \to X_s e^+ e^-$ in the q_3^2 bin. Top row left is the $m_{\rm ES}$ fit projection, top row right is the L_R fit projection; middle row left is a signal-enhanced $m_{\rm ES}$ fit projection for events with $L_R > 0.8$, middle row right is a signal-enhanced L_R fit projection for events in the $m_{\rm ES} > 5.27\,{\rm GeV}/c^2$ signal region. The lower left hand plot is the profile likelihood curve for the 2D data fit.

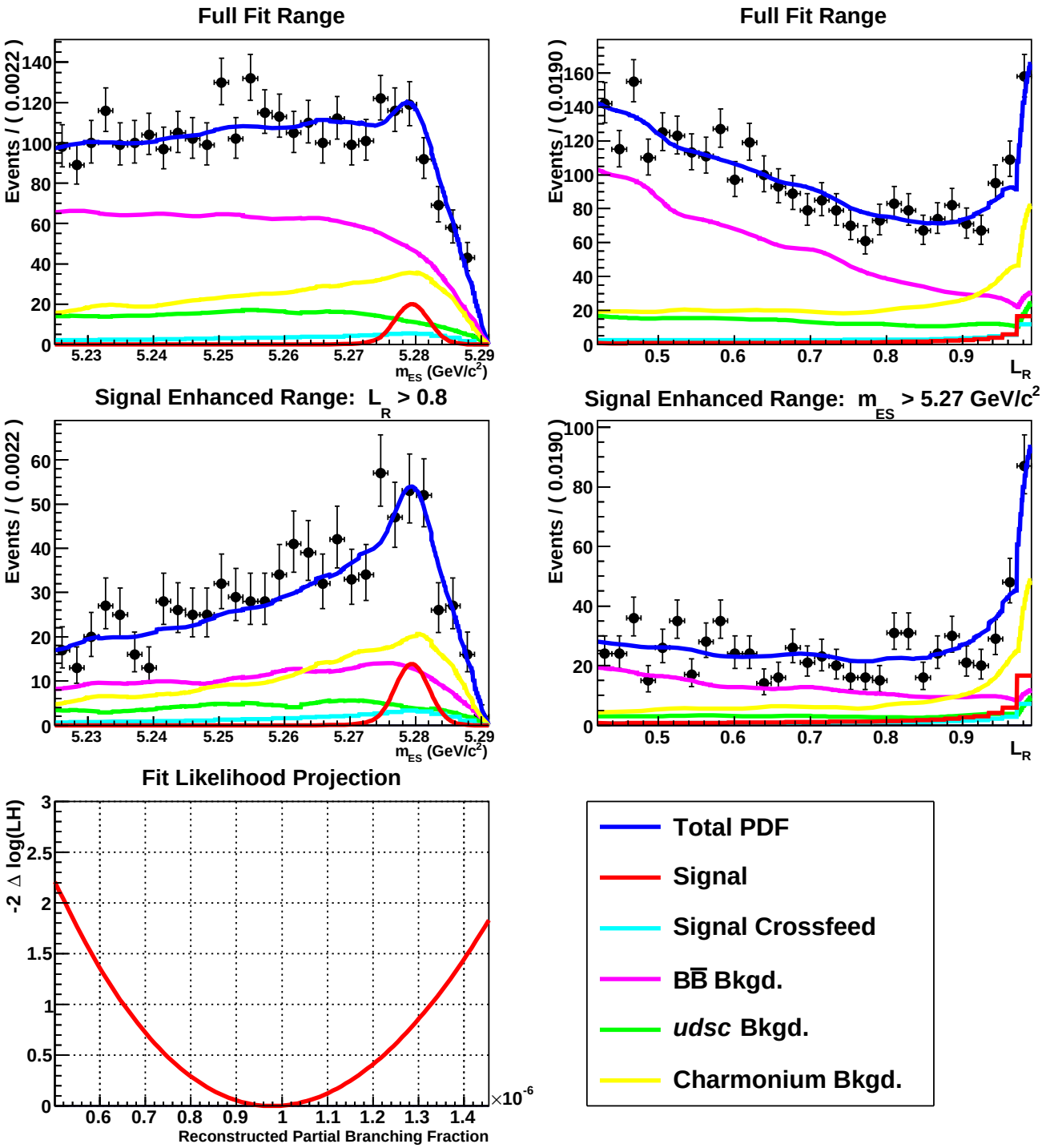

FIG. 8: Fit to $B \to X_s\, e^+ e^-$ in the q_4^2 bin. Top row left is the $m_{\rm ES}$ fit projection, top row right is the L_R fit projection; middle row left is a signal-enhanced $m_{\rm ES}$ fit projection for events with $L_R > 0.8$, middle row right is a signal-enhanced L_R fit projection for events in the $m_{\rm ES} > 5.27\,{\rm GeV}/c^2$ signal region. The lower left hand plot is the profile likelihood curve for the 2D data fit.

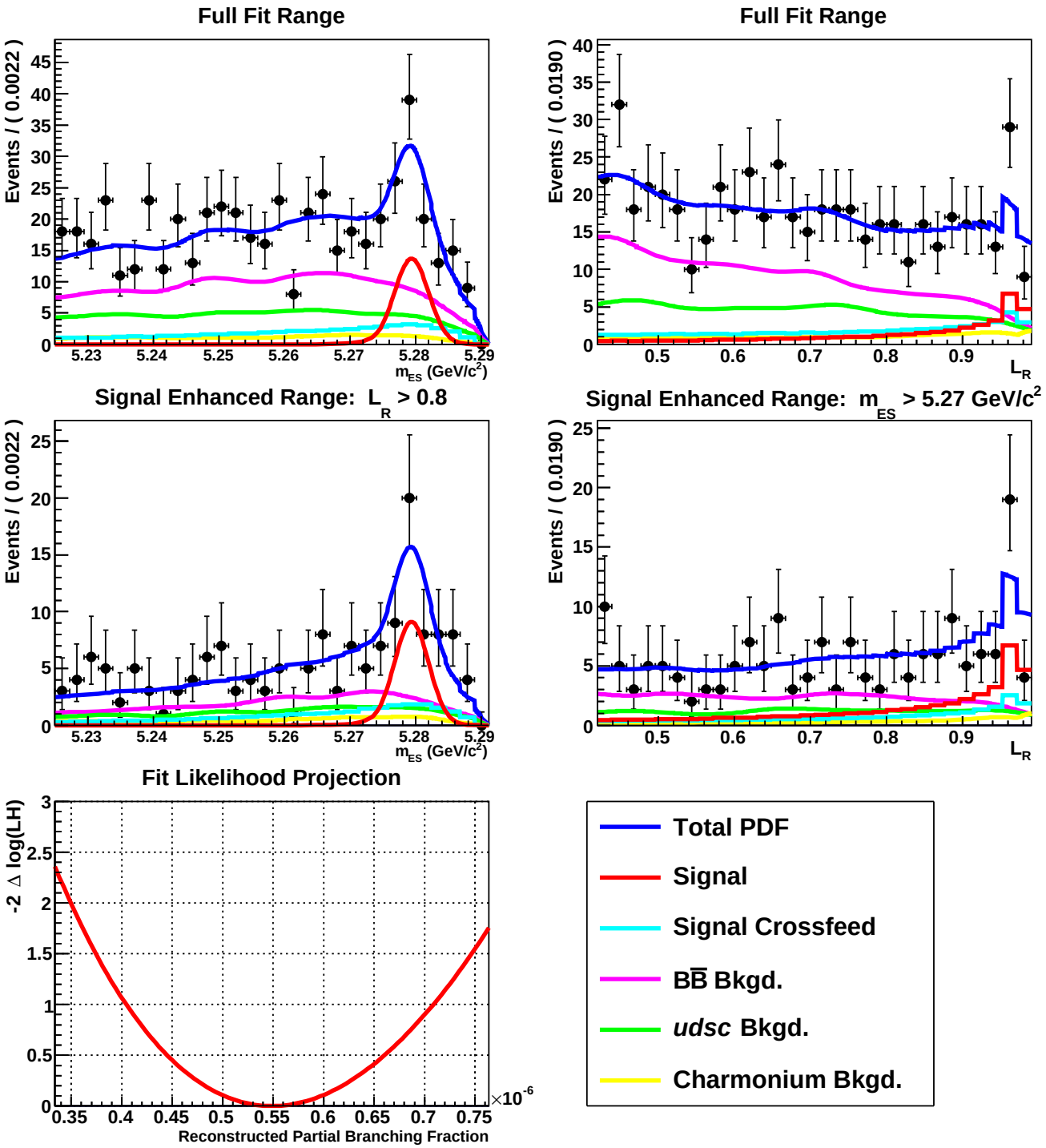

FIG. 9: Fit to $B \to X_s e^+ e^-$ in the q_5^2 bin. Top row left is the $m_{\rm ES}$ fit projection, top row right is the L_R fit projection; middle row left is a signal-enhanced $m_{\rm ES}$ fit projection for events with $L_R > 0.8$, middle row right is a signal-enhanced L_R fit projection for events in the $m_{\rm ES} > 5.27\,{\rm GeV}/c^2$ signal region. The lower left hand plot is the profile likelihood curve for the 2D data fit.

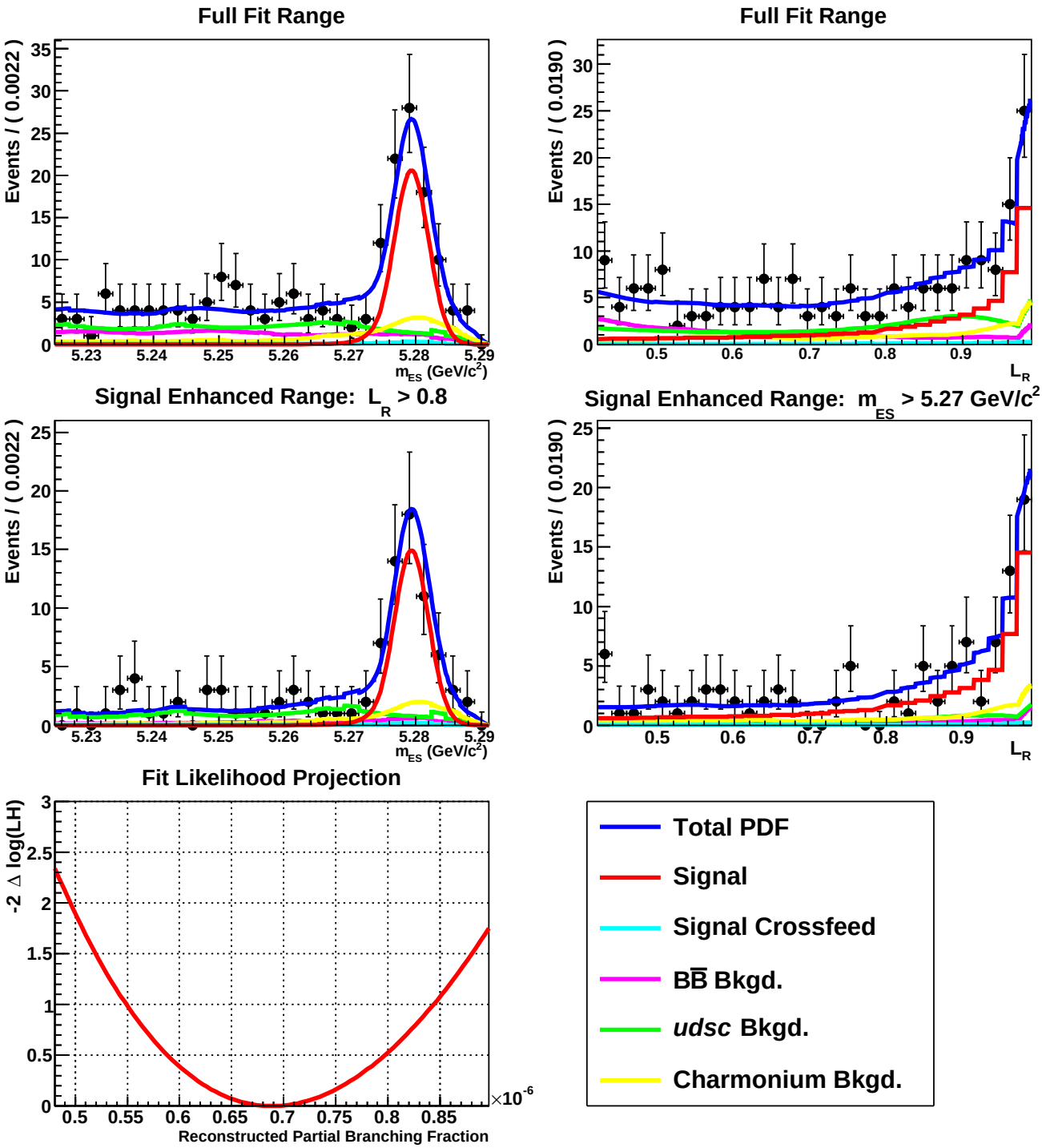

FIG. 10: Fit to $B \to X_s\, e^+ e^-$ in the $m_{X_s,1}$ bin. Top row left is the $m_{\rm ES}$ fit projection, top row right is the L_R fit projection; middle row left is a signal-enhanced $m_{\rm ES}$ fit projection for events with $L_R > 0.8$, middle row right is a signal-enhanced L_R fit projection for events in the $m_{\rm ES} > 5.27\,{\rm GeV}/c^2$ signal region. The lower left hand plot is the profile likelihood curve for the 2D data fit.

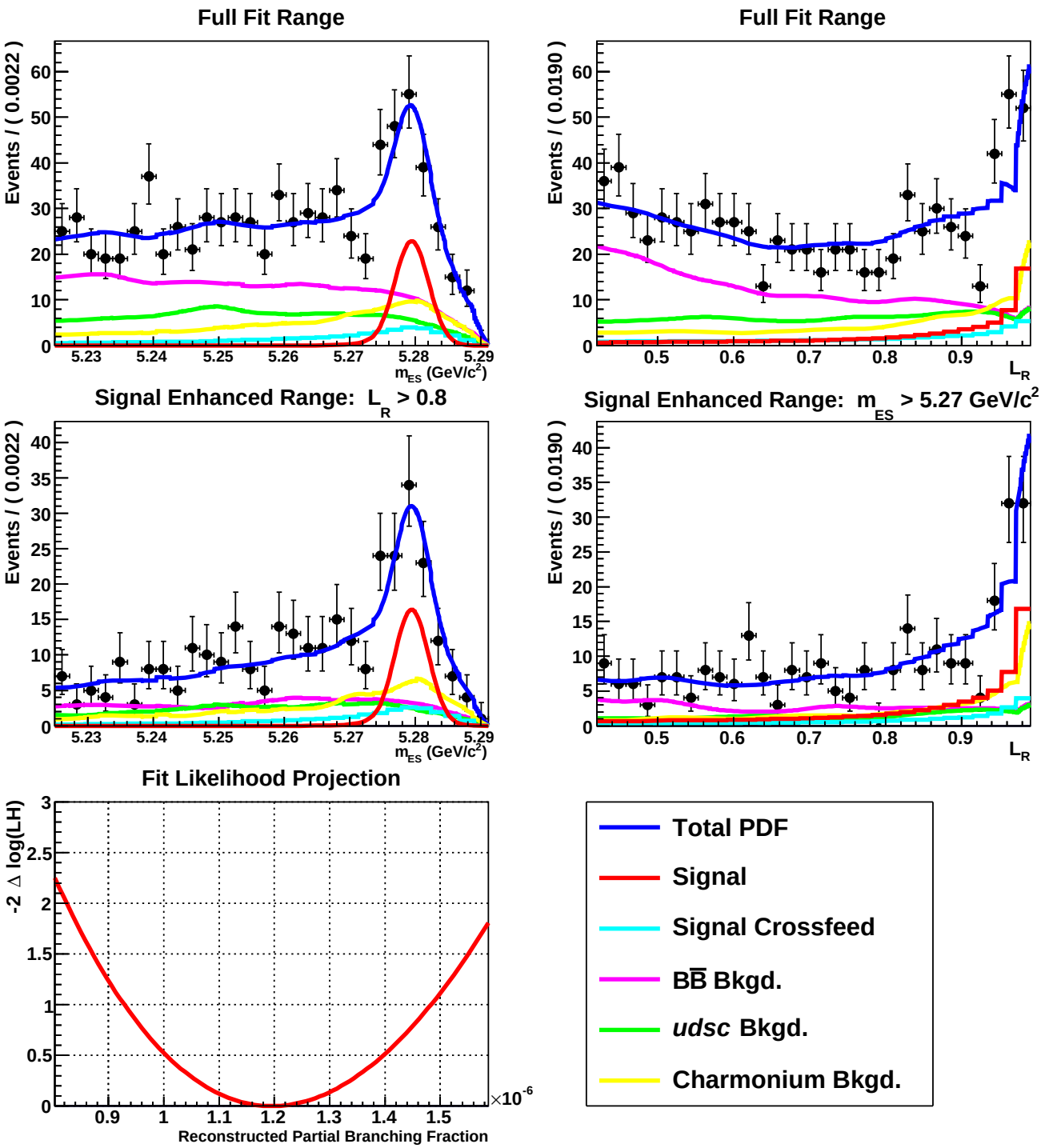

FIG. 11: Fit to $B \to X_s\, e^+ e^-$ in the $m_{X_s,2}$ bin. Top row left is the $m_{\rm ES}$ fit projection, top row right is the L_R fit projection; middle row left is a signal-enhanced $m_{\rm ES}$ fit projection for events with $L_R > 0.8$, middle row right is a signal-enhanced L_R fit projection for events in the $m_{\rm ES} > 5.27\,{\rm GeV}/c^2$ signal region. The lower left hand plot is the profile likelihood curve for the 2D data fit.

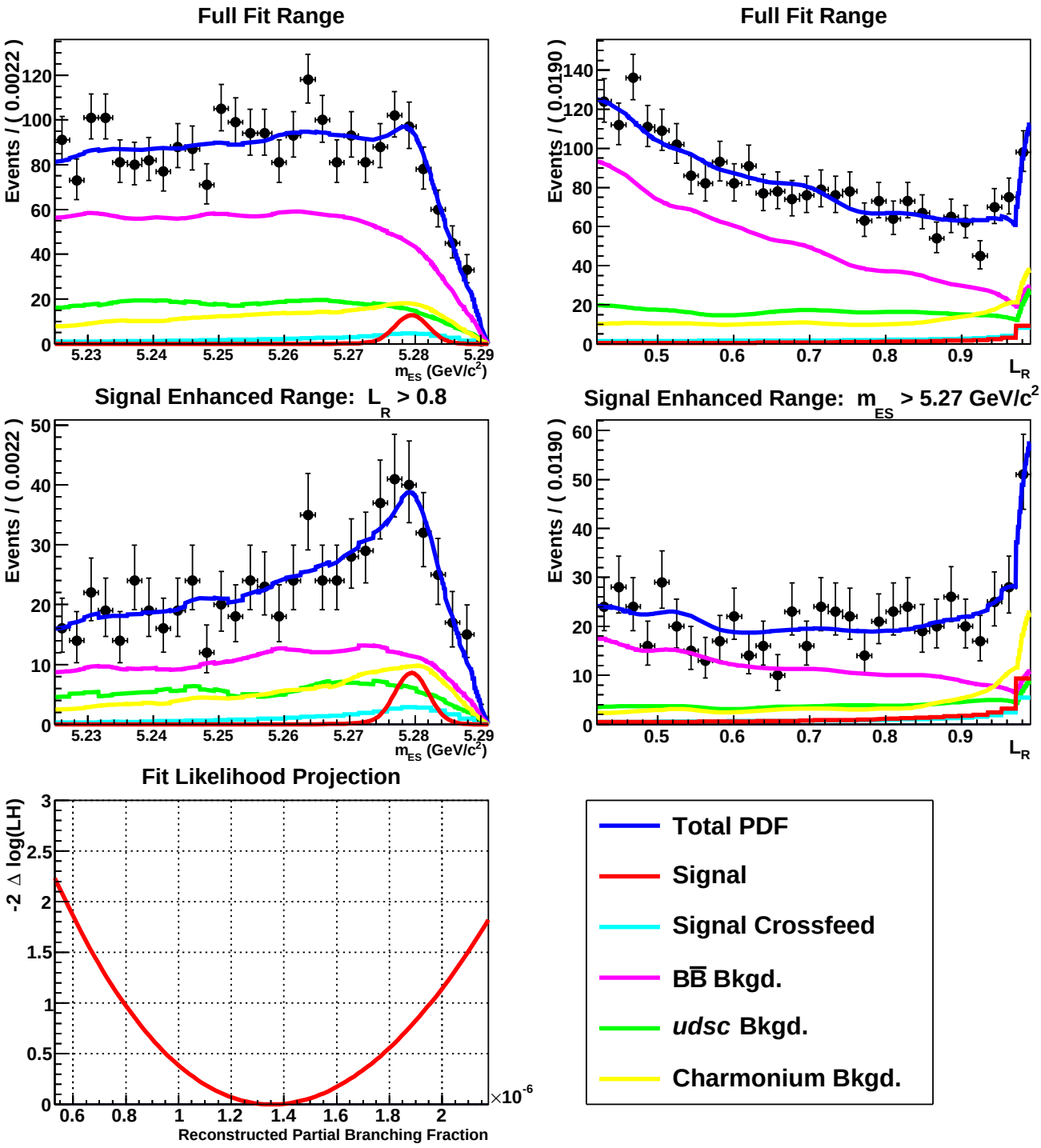

FIG. 12: Fit to $B \to X_s\, e^+ e^-$ in the $m_{X_s,3}$ bin. Top row left is the $m_{\rm ES}$ fit projection, top row right is the L_R fit projection; middle row left is a signal-enhanced $m_{\rm ES}$ fit projection for events with $L_R > 0.8$, middle row right is a signal-enhanced L_R fit projection for events in the $m_{\rm ES} > 5.27\,{\rm GeV}/c^2$ signal region. The lower left hand plot is the profile likelihood curve for the 2D data fit.

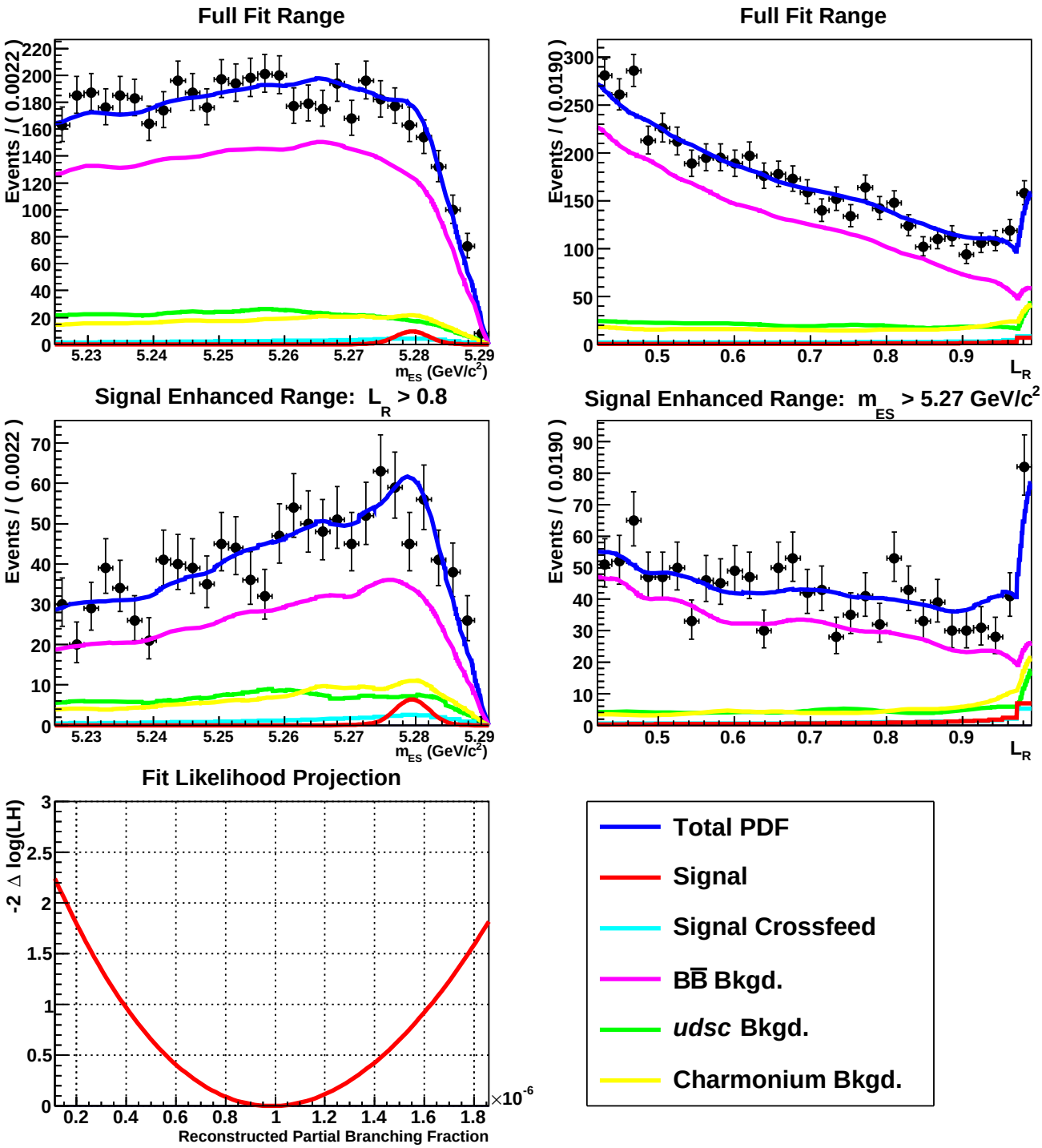

FIG. 13: Fit to $B \to X_s\, e^+ e^-$ in the $m_{X_s,4}$ bin. Top row left is the $m_{\rm ES}$ fit projection, top row right is the L_R fit projection; middle row left is a signal-enhanced $m_{\rm ES}$ fit projection for events with $L_R > 0.8$, middle row right is a signal-enhanced L_R fit projection for events in the $m_{\rm ES} > 5.27\,{\rm GeV}/c^2$ signal region. The lower left hand plot is the profile likelihood curve for the 2D data fit.

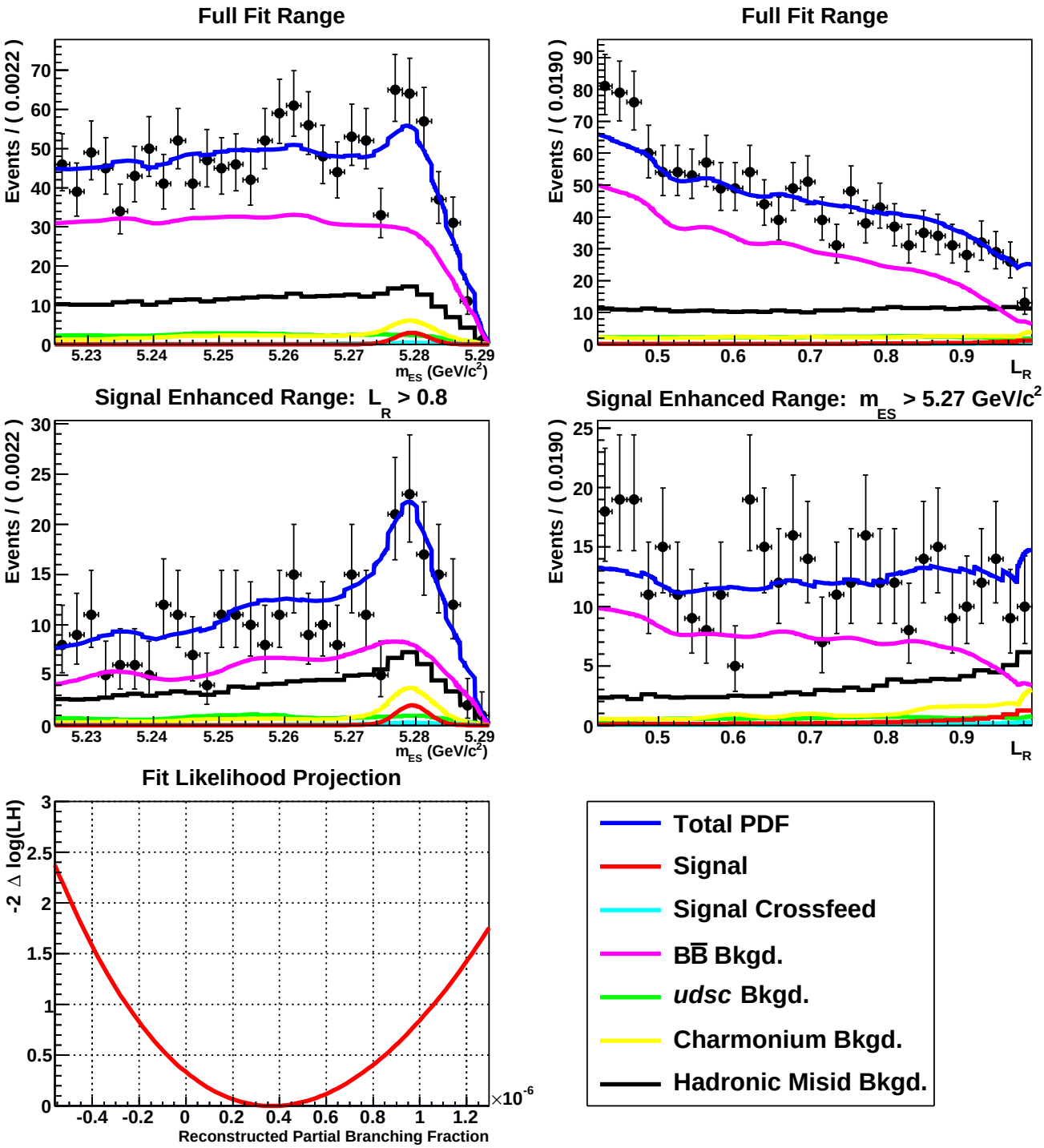

FIG. 14: Fit to $B \to X_s\,\mu^+\mu^-$ in the q_0^2 bin. Top row left is the $m_{\rm ES}$ fit projection, top row right is the L_R fit projection; middle row left is a signal-enhanced $m_{\rm ES}$ fit projection for events with $L_R > 0.8$, middle row right is a signal-enhanced L_R fit projection for events in the $m_{\rm ES} > 5.27\,{\rm GeV}/c^2$ signal region. The lower left hand plot is the profile likelihood curve for the 2D data fit.

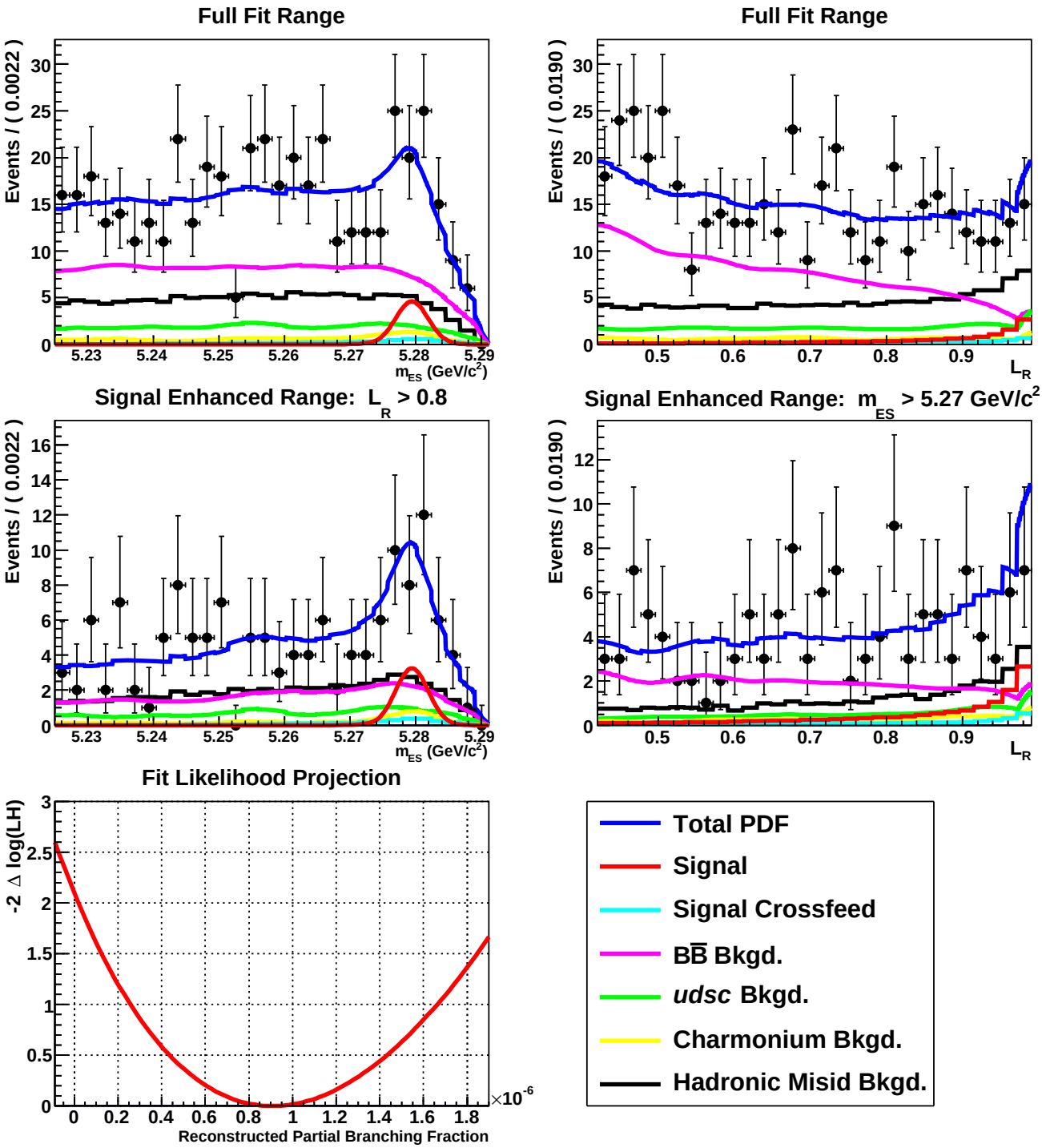

FIG. 15: Fit to $B \to X_s\,\mu^+\mu^-$ in the q_1^2 bin. Top row left is the $m_{\rm ES}$ fit projection, top row right is the L_R fit projection; middle row left is a signal-enhanced $m_{\rm ES}$ fit projection for events with $L_R > 0.8$, middle row right is a signal-enhanced L_R fit projection for events in the $m_{\rm ES} > 5.27\,{\rm GeV}/c^2$ signal region. The lower left hand plot is the profile likelihood curve for the 2D data fit.

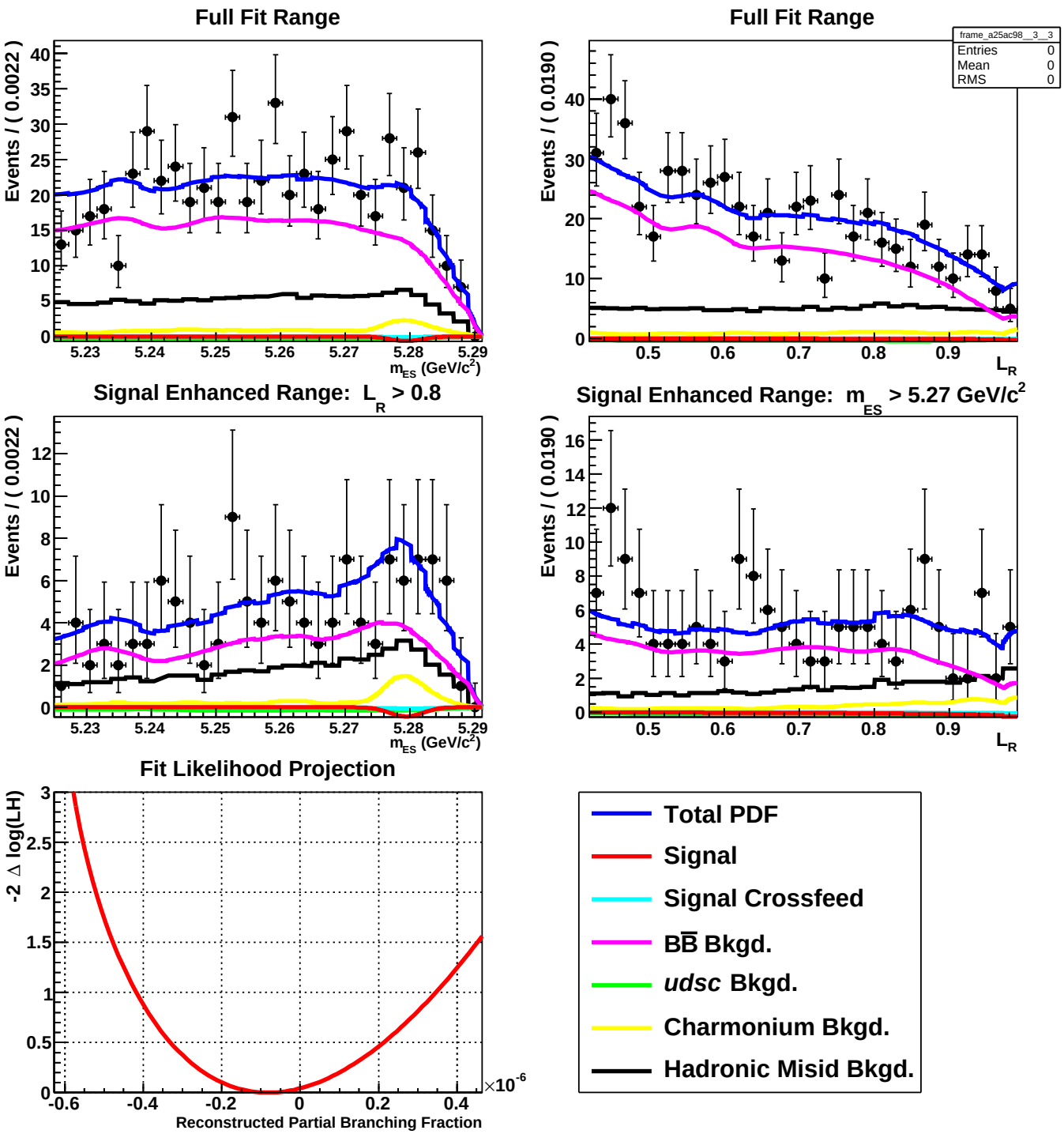

FIG. 16: Fit to $B \to X_s\,\mu^+\mu^-$ in the q_2^2 bin. Top row left is the $m_{\rm ES}$ fit projection, top row right is the L_R fit projection; middle row left is a signal-enhanced $m_{\rm ES}$ fit projection for events with $L_R > 0.8$, middle row right is a signal-enhanced L_R fit projection for events in the $m_{\rm ES} > 5.27\,{\rm GeV}/c^2$ signal region. The lower left hand plot is the profile likelihood curve for the 2D data fit.

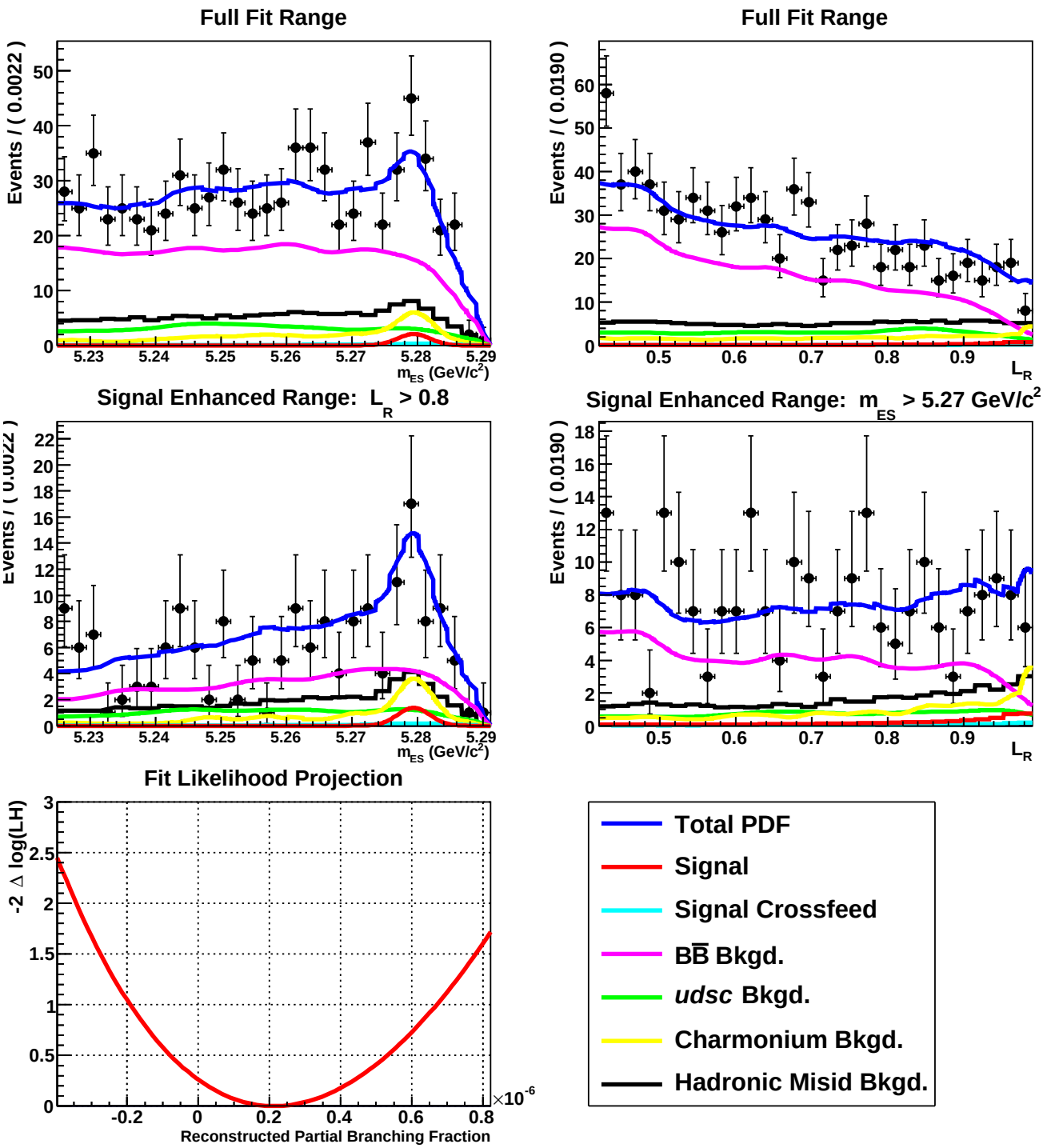

FIG. 17: Fit to $B \to X_s\,\mu^+\mu^-$ in the q_3^2 bin. Top row left is the $m_{\rm ES}$ fit projection, top row right is the L_R fit projection; middle row left is a signal-enhanced $m_{\rm ES}$ fit projection for events with $L_R > 0.8$, middle row right is a signal-enhanced L_R fit projection for events in the $m_{\rm ES} > 5.27\,{\rm GeV}/c^2$ signal region. The lower left hand plot is the profile likelihood curve for the 2D data fit.

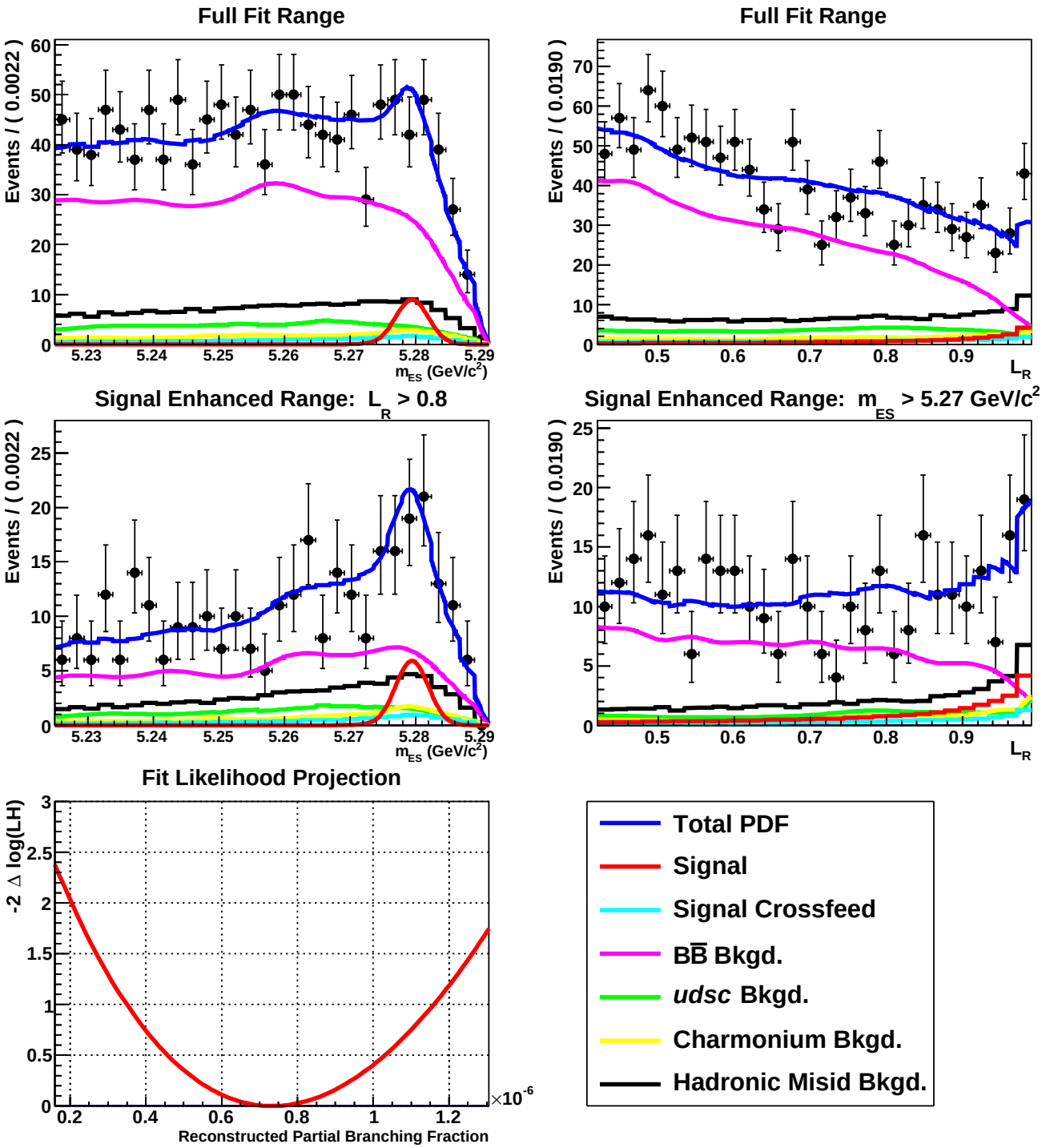

FIG. 18: Fit to $B \to X_s\,\mu^+\mu^-$ in the q_4^2 bin. Top row left is the $m_{\rm ES}$ fit projection, top row right is the L_R fit projection; middle row left is a signal-enhanced $m_{\rm ES}$ fit projection for events with $L_R > 0.8$, middle row right is a signal-enhanced L_R fit projection for events in the $m_{\rm ES} > 5.27\,{\rm GeV}/c^2$ signal region. The lower left hand plot is the profile likelihood curve for the 2D data fit.

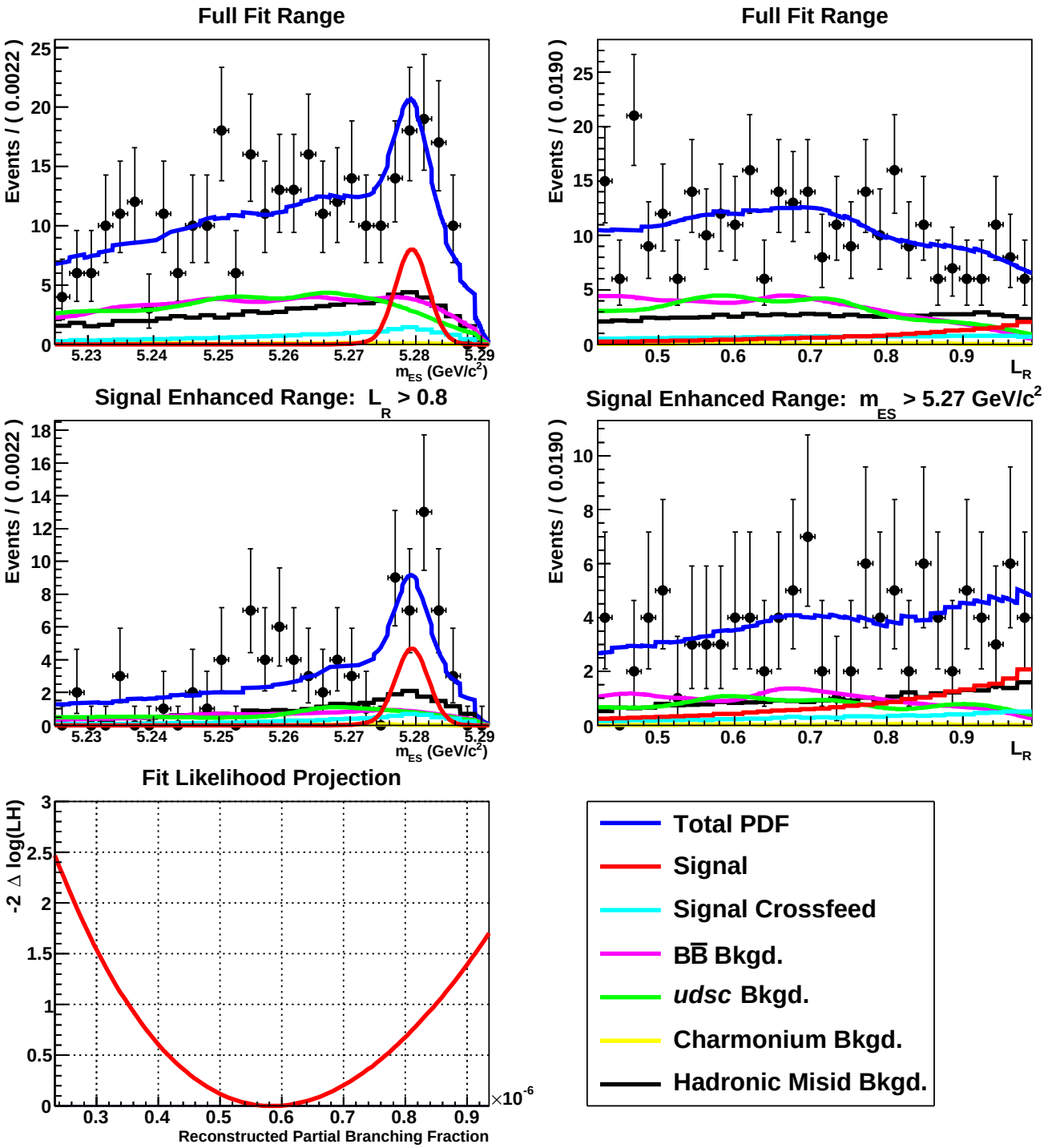

FIG. 19: Fit to $B \to X_s\,\mu^+\mu^-$ in the q^2_5 bin. Top row left is the $m_{\rm ES}$ fit projection, top row right is the L_R fit projection; middle row left is a signal-enhanced $m_{\rm ES}$ fit projection for events with $L_R > 0.8$, middle row right is a signal-enhanced L_R fit projection for events in the $m_{\rm ES} > 5.27\,{\rm GeV}/c^2$ signal region. The lower left hand plot is the profile likelihood curve for the 2D data fit.

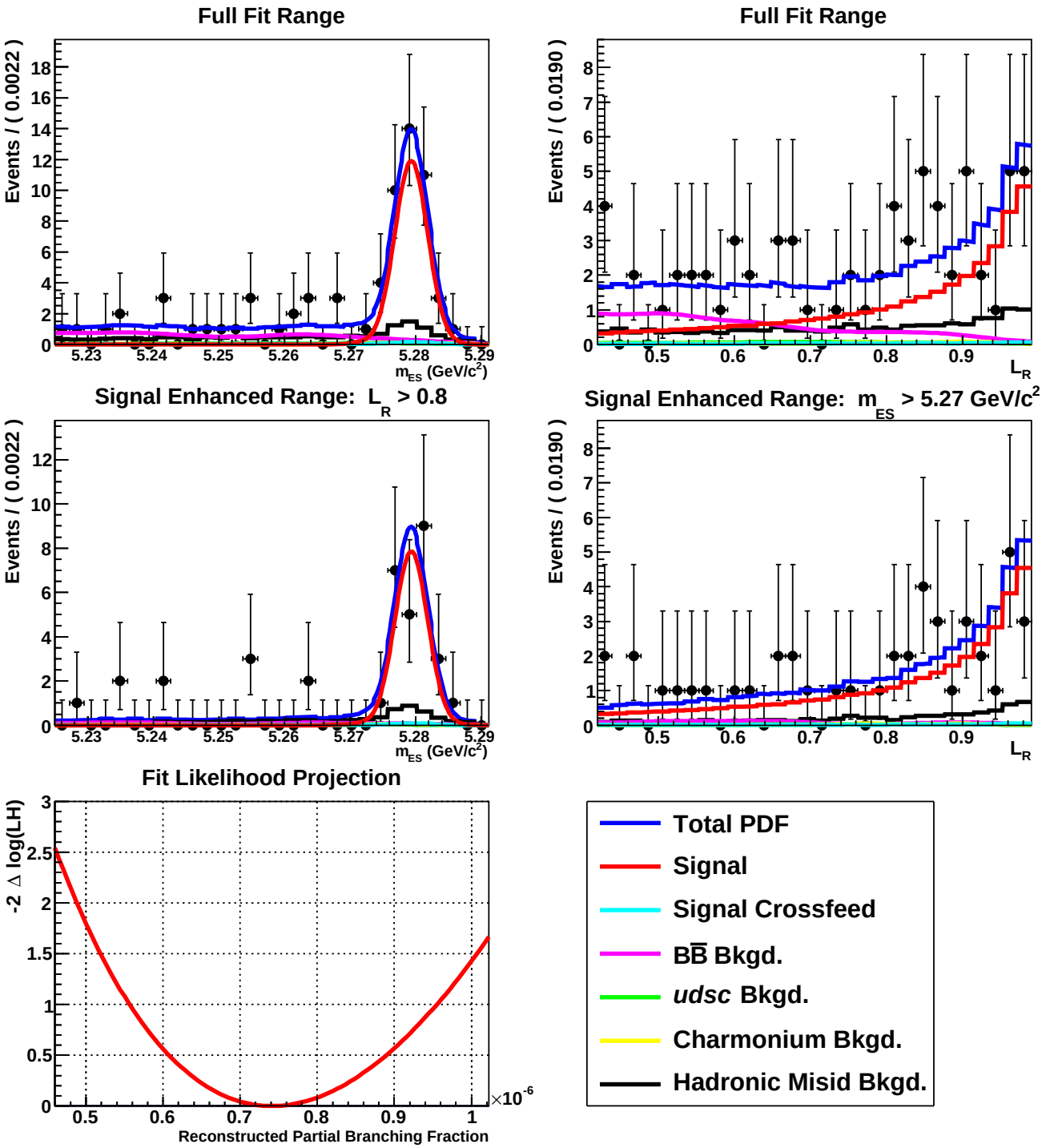

FIG. 20: Fit to $B \to X_s\,\mu^+\mu^-$ in the $m_{X_s,1}$ bin. Top row left is the $m_{\rm ES}$ fit projection, top row right is the L_R fit projection; middle row left is a signal-enhanced $m_{\rm ES}$ fit projection for events with $L_R > 0.8$, middle row right is a signal-enhanced L_R fit projection for events in the $m_{\rm ES} > 5.27\,{\rm GeV}/c^2$ signal region. The lower left hand plot is the profile likelihood curve for the 2D data fit.

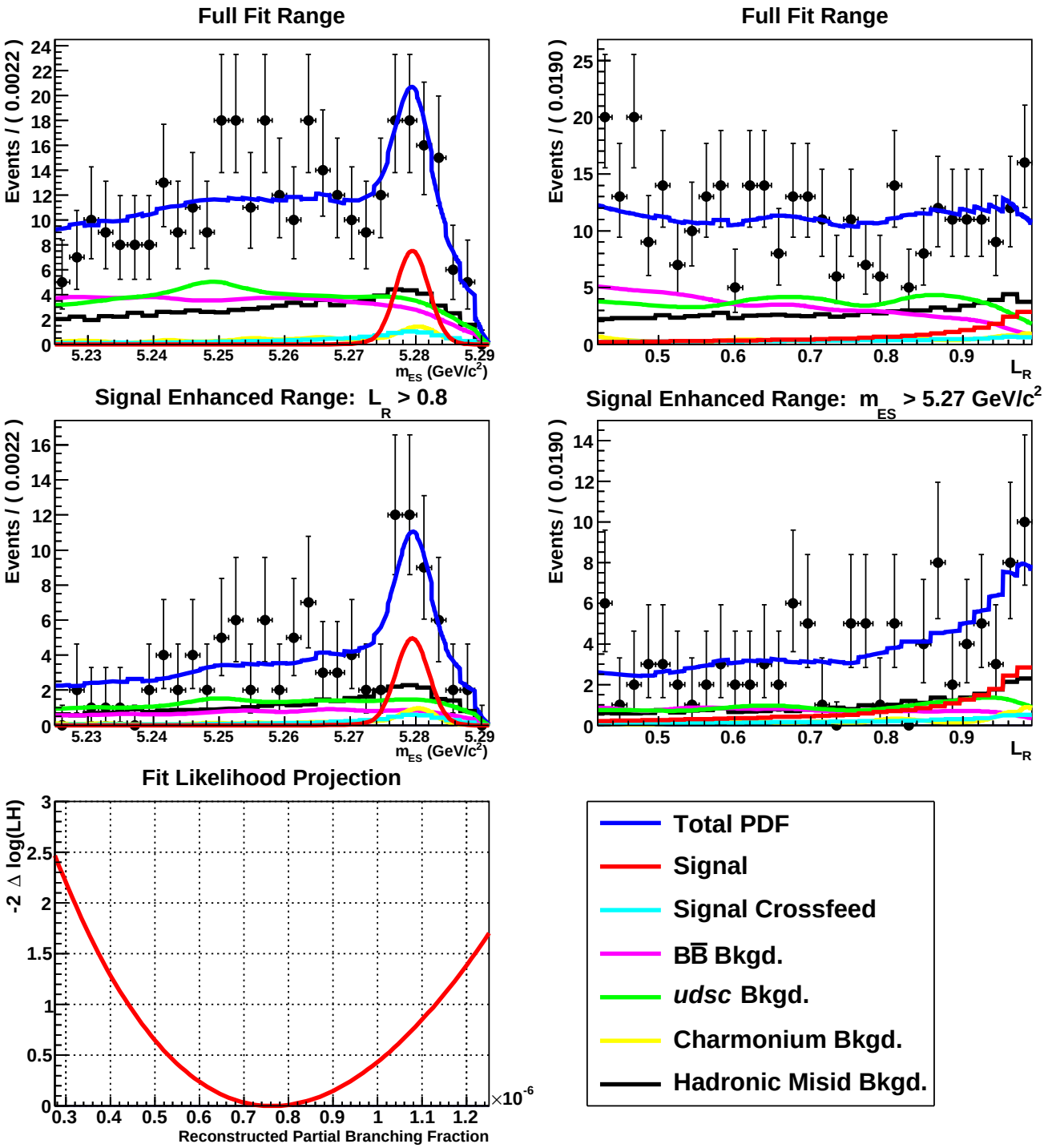

FIG. 21: Fit to $B \to X_s\,\mu^+\mu^-$ in the $m_{X_s,2}$ bin. Top row left is the $m_{\rm ES}$ fit projection, top row right is the L_R fit projection; middle row left is a signal-enhanced $m_{\rm ES}$ fit projection for events with $L_R > 0.8$, middle row right is a signal-enhanced L_R fit projection for events in the $m_{\rm ES} > 5.27\,{\rm GeV}/c^2$ signal region. The lower left hand plot is the profile likelihood curve for the 2D data fit.

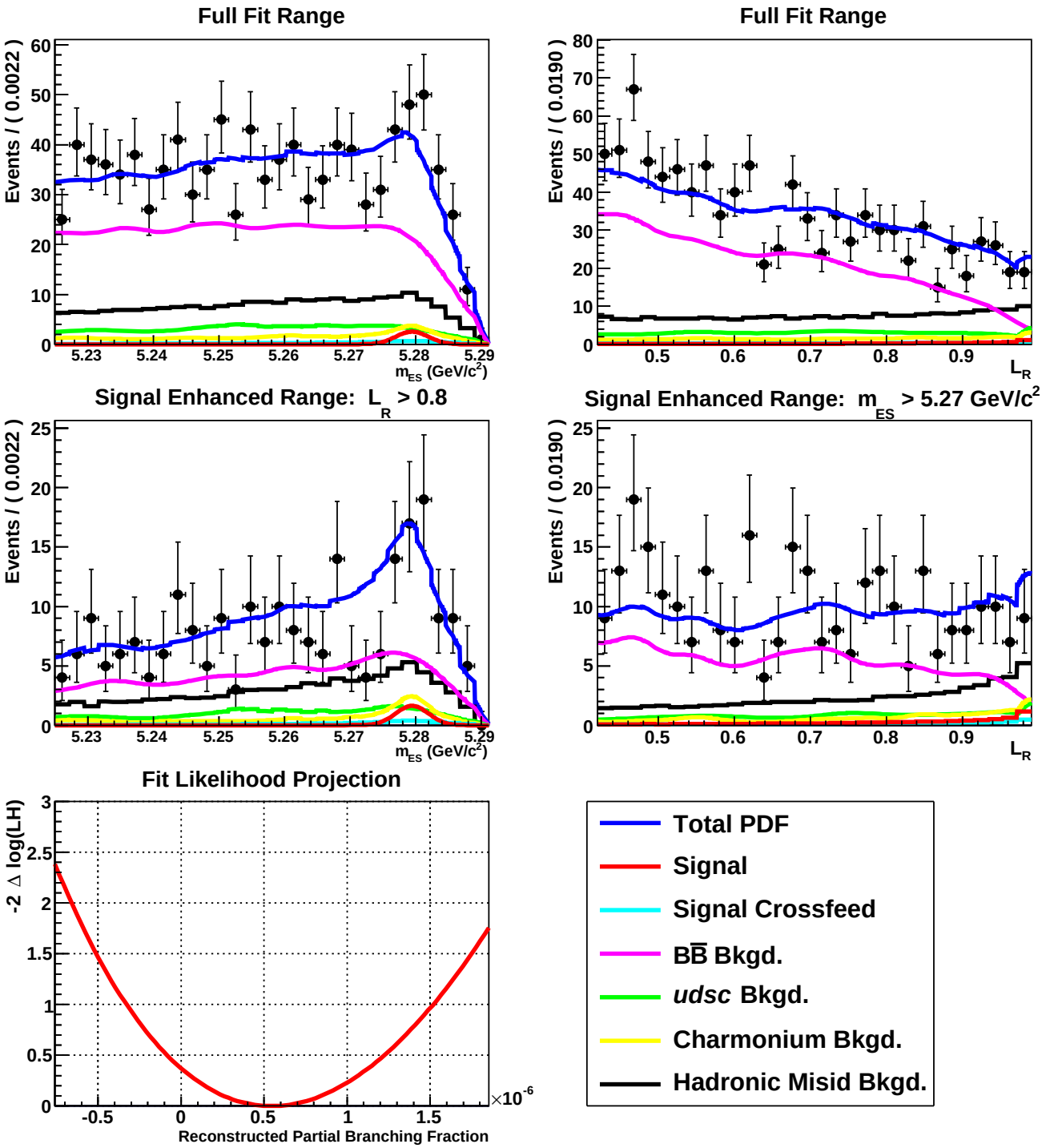

FIG. 22: Fit to $B \to X_s\,\mu^+\mu^-$ in the $m_{X_s,3}$ bin. Top row left is the $m_{\rm ES}$ fit projection, top row right is the L_R fit projection; middle row left is a signal-enhanced $m_{\rm ES}$ fit projection for events with $L_R > 0.8$, middle row right is a signal-enhanced L_R fit projection for events in the $m_{\rm ES} > 5.27\,{\rm GeV}/c^2$ signal region. The lower left hand plot is the profile likelihood curve for the 2D data fit.

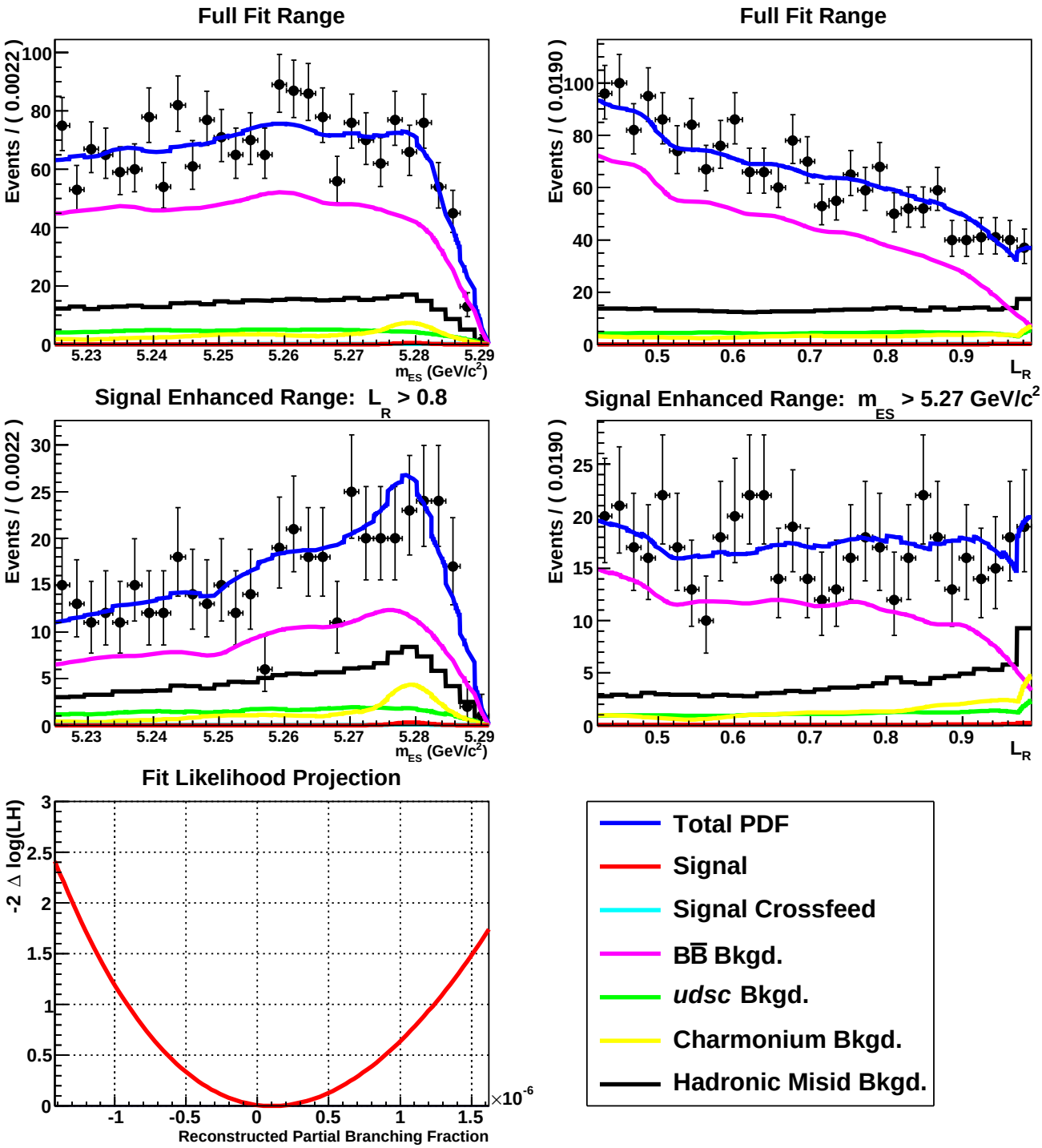

FIG. 23: Fit to $B \to X_s\,\mu^+\mu^-$ in the $m_{X_s,4}$ bin. Top row left is the $m_{\rm ES}$ fit projection, top row right is the L_R fit projection; middle row left is a signal-enhanced $m_{\rm ES}$ fit projection for events with $L_R > 0.8$, middle row right is a signal-enhanced L_R fit projection for events in the $m_{\rm ES} > 5.27\,{\rm GeV}/c^2$ signal region. The lower left hand plot is the profile likelihood curve for the 2D data fit.